Pure & Appl. Chem., Vol.52, pp.571-605. 0033-4545/80/0301-0571$02.00/0
Pergamon Press Ltd. 1980. Printed in Great Britain.

THE ROLE OF ELECTRON TRANSFER AND CHARGE TRANSFER IN ORGANOMETALLIC CHEMISTRY

Jay K. Kochi

Department of Chemistry, Indiana University, Bloomington, Indiana 47405

Abstract - The principal objective of this lecture is to describe the efficacy of organometals as electron donors, and to show how this property dominates many aspects of their chemistry. First, the structural effects of alkyl ligands (R) on the highest occupied molecular orbital (HOMO) of the neutral alkylmetals, R_4Sn, R_4Pb and R_2Hg, are probed by photoelectron spectroscopy. The chemical properties of the resultant paramagnetic cation is then discussed. Electron transfer from alkylmetals to iron(III) complexes is shown to proceed via an outer-sphere mechanism, whereas that to iridate(IV) and tetracyanoethylene are inner-sphere processes. The difference lies in their response to steric effects in the alkylmetals. Steric effects are quantitatively evaluated with the aid of charge transfer transition energies in the absorption spectra of alkylmetal-tetracyanoethylene complexes. After correction for the steric effect, the rates of electron transfer from alkylmetal to both hexachloroiridate(IV) and tetracyanoethylene follow a linear free energy relationship with a Brönsted slope $\alpha = 1$, predicted by Marcus theory for inner-sphere mechanisms. The generalized concept of charge transfer is applied to a variety of organonickel systems, including (1) the oxidative addition of aryl halides to triethylphosphinenickel(0) complexes, (2) biaryl synthesis from the induced decomposition of arylnickel(II) halides, (3) oxygen atom transfer from organic nitro compounds to coordinated phosphines in nickel(0) complexes and finally even to (4) π-ligand substitution of benzophenones into phosphinenickel(0) complexes.

INTRODUCTION

Interest in organometallic chemistry stems in large part from the wide variety of reactions which allow for their use, either as reactants or as intermediates, in synthetic procedures. Some typical examples of reactions involving organometals are:

Addition:

$$RMgX + \diagup C{=}O \longrightarrow R\overset{|}{C}OMgX$$

Reduction:

$$HSnR_3 + \diagup C{=}C\diagdown \longrightarrow H\overset{|}{C}\overset{|}{C}SnR_3$$

Halogenolysis:

$$R_3B + Br_2 \longrightarrow R_2BBr + RBr$$

Oxidative Addition:

$$RAuL + RX \longrightarrow \overset{R}{\underset{X}{R\text{-}Au\text{-}L}}$$

Reductive Elimination:

$$L_2PtR_2 \longrightarrow RH + R(\text{-}H) + [L_2Pt]$$

Coupling:

$$L_2FeR_2^+ \longrightarrow R\text{-}R + [L_2Fe^+]$$

Insertion:

$$CpFe(CO)_2R + SO_2 \longrightarrow CpFe(CO)_2OSOR$$

Carbonylation:

$$Fe(CO)_4^{2-} + RX \longrightarrow RCOFe(CO)_4^-$$

Autoxidation:

$$CH_3Co(chel) + O_2 \longrightarrow CH_3OOCo(chel)$$

Alkylation:

Oxygen Transfer:

$$R_3SiSiR_3 + PhCO_3H \longrightarrow R_3SiOSiR_3 + PhCO_2H$$

The diversity of these transformations presents a mechanistic challenge, since in each process, it is not clear how the bond between the metal center and the carbon-containing ligand is formed or how it is broken. Is there a common chemical property among the reagents listed which allow for facile reaction? Some of them are classical electrophiles such as the acids, halogens, tetracyanoethylene, etc. Others, like oxygen and iron(III), are more properly considered to be oxidants. Moreover, the organic halides and carbonyl compounds are difficult to classify.

In this presentation I would like to address these questions by considering first the stability of organometals and then focus on their properties as electron donors. Paramagnetic ion-radicals of organometals are central to our discussion, and their behavior will be reviewed briefly. Most importantly, the nature of electron transfer and charge transfer processes as they apply to organometals as electron donors will be carefully delineated. Finally, we wish to describe the general applicability of electron transfer and charge transfer mechanisms to a variety of organometallic reactions of nickel.

I. STABILITY OF ORGANOMETALS

A number of alkylmetals especially of the main group elements are known as quite stable compounds. For homolytic decomposition,

$$R_nM(g) \longrightarrow M(g) + nR\cdot(g) \qquad \Delta H^\circ/n = \overline{D}(R\text{-}M)$$

the mean bond dissociation energy $\overline{D}(R\text{-}M)$ for binary alkylmetals such as those given in Table I can be obtained from the enthalpy of formation of the alkylmetal in conjunction with

Table I. Mean Bond Dissociation Energies of Organometals.

$LiCH_3$	59	$C(CH_3)_4$	87	$Ta(CH_3)_5$	62
$Mg(CH_3)_2$	38	$Si(CH_3)_4$	77	$W(CH_3)_6$	38
$Zn(CH_3)_2$	44	$Ge(CH_3)_4$	65	$(CO)_5MnCH_3$	30
$Hg(CH_3)_2$	30	$Sn(CH_3)_4$	54	$Ti(CH_2CMe_3)_4$	50
$B(CH_3)_3$	89	$Pb(CH_3)_4$	40	$Zr(CH_2CMe_3)_4$	60
$Al(CH_3)_3$	62			$Hf(CH_2CMe_3)_4$	64

the enthalpies of formation of the alkyl radicals and gaseous metal atoms, i.e.,(1)

$$n\overline{D}(R\text{-}M) = \Delta H^\circ = \Delta H_f^\circ M(g) + n\,\Delta H_f^\circ R\cdot(g) - \Delta H_f^\circ MR_n(g)$$

However, these mean bond dissociation energies usually differ significantly from the individual bond energies D_i,

$$R_nM \longrightarrow R\cdot + R_{n-1}M \qquad \Delta H_1 = D_1$$

$$R_{n-1}M \longrightarrow R\cdot + R_{n-2}M \text{ , etc.} \qquad \Delta H_2 = D_2$$

where $\Sigma D_i = n\overline{D}$. Indeed, it has been found that D_1 is much larger than D_2 in dichloromercury(II) as shown in Table II. Similarly, the first bond dissociation energies for CH_3-HgCl

Table II. Bond Energies (kcal mol^{-1}) in Mercurials.

Hg Compound	$D_1 + D_2$	D_1	D_2
Cl-HgCl	106	81	24
CH_3-HgCl		64±2	
CH_3-$HgCH_3$	58±2	51±2	7±3 (diff.)

and CH_3-$HgCH_3$ are significantly larger than the second D_2. In these examples, the differences in bond energies reflect the relative stabilities of diamagnetic mercury(II) complexes compared to the paramagnetic mercury(I) derivatives.

From these illustrations, it is clear that paramagnetic organometal species are much more prone to undergo reaction than their diamagnetic precursors.

II. ORGANOMETALS AS ELECTRON DONORS

We now turn our attention to paramagnetic species formed by electron loss from the organometal, i.e., the organometal cation-radical. Such radical-cations are generated in the gas phase by photoionization, e.g.,(2)

$$CH_3HgCH_3 \xrightarrow{h\nu} CH_3HgCH_3^+ + \epsilon \qquad (1)$$

Importantly, the use of monochromatic photons, such as those from the 584 Å resonance line of a helium discharge lamp, is the basis for the photoelectron spectroscopic (pes) determination of the ionization potentials of many organometals. The latter is particularly useful for probing the effects of ligand structure. For example, the He(I) photoelectron spectra of dialkylmercury compounds show two principal bands of interest. The first vertical ionization potential, lying in a rather wide range between 7.57 eV (t-Bu_2Hg) and 9.33 eV (Me_2Hg), is included in a broad unsymmetrical band. A second, weaker band occurring between 14.4 and 15.0 eV is due to ionization from the mercury $5d^{10}$ shell. The effect of alkyl substitution on the first and second ionization potentials of dialkylmercury(II) compounds is indicated in Table III. The plot in Figure 1 shows the effect of alkyl structure on

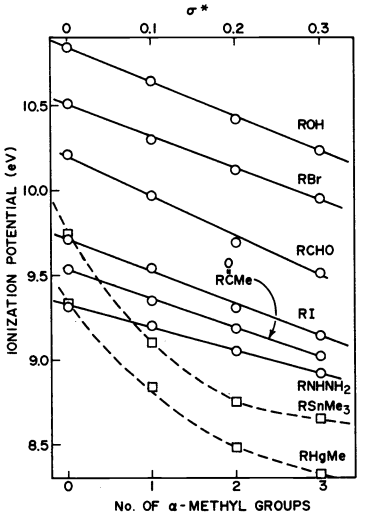

Figure 1. Effect of alkyl structure on the ionization potentials of organometals, and their comparison with other organic derivatives.

the ionization potentials of a series of homologous $RHgCH_3$, in which R represents increasing α-branching in the order: CH_3, CH_3CH_2, $(CH_3)_2CH$ and $(CH_3)_3C$. It is particularly noteworthy that the ionization potential decreases by more than 20 kcal mol^{-1} simply by replacing one methyl group in Me_2Hg with a t-butyl group. Such a large electronic effect occurs even without directly altering the nature of the bonding to the mercury center, and it

Table III. Photoelectron Spectra of Tetraalkyltin Compounds.

	SnR_4	$\Sigma\sigma^*$	IP_1 (eV)			$\overline{IP}$ (eV)
1	Me	0	9.7			9.7
2	Et	.40	8.93			8.93
3	n-Pr	.46	8.82			8.82
4	i-Pr	.76	8.46			8.46
5	n-Bu	.52	8.76			8.76
6	i-Bu	.50	8.68			8.68
7	s-Bu	.84	8.45			8.45
8	neo-Pentyl	.66	8.67			8.67
	Me_2SnR_2	$\Sigma\sigma^*$	IP_1	IP_2	IP_3	
9	Et	.20	9.01	9.28	9.64	9.31
10	n-Pr	.23	8.8	9.2	9.5	9.17
11	i-Pr	.38	8.56	8.99	9.55	9.03
12	n-Bu	.26	8.8	9.2	9.5	9.17
13	t-Bu	.6	8.22	8.74	9.47	8.81
	Me_3SnR	$\Sigma\sigma^*$	IP_1	IP_2		
14	Et	.10	9.1	9.5		9.37
15	n-Pr	.115	9.1	-		-
16	i-Pr	.19	8.9	9.45, 9.76		9.37
17	n-Bu	.13	9.0	9.49		9.33
18	i-Bu	.125	9.05	9.50		9.35
19	t-Bu	.30	8.50	9.62		9.24
20	Et_3MeSn	.30	8.95	9.3		9.07

emphasizes the importance of the donor property of alkyl ligands on the redox properties of metal complexes. The ionization process in organometals such as Me_2Hg proceeds from a molecular orbital (HOMO) that has substantial metal-carbon bonding characteristics as qualitatively portrayed in the simple linear combination of group orbital diagram:

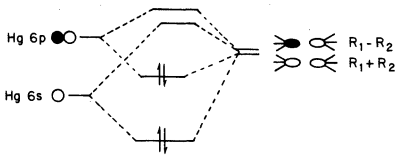

Indeed, the ionization of alkyl radicals [i.e., $R\cdot \rightarrow R^+ + \epsilon$] serves as a reasonable model for the ionization from the HOMO of organomercurials as shown in Figure 2.

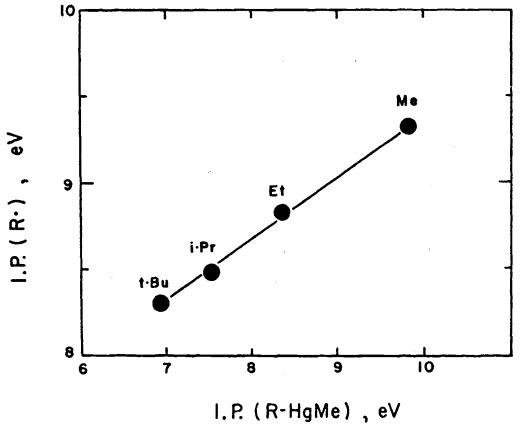

Figure 2. Structural relationships in the oxidation potentials of alkyl radicals and alkylmercury compounds (see Table III for numbering of compounds).

Essentially the same conclusion derives from the examination of the pes of the tetraalkylmetals of the Group IVA elements. Thus the vertical ionization potentials of the tetramethyl derivatives, CMe_4, $SiMe_4$, $GeMe_4$, $SnMe_4$ and $PbMe_4$ decrease monotonically in the order: 10.96, 10.57, 10.23, 9.70 and 8.81 eV, respectively,(3) indicating that ionization is associated with electrons localized relatively close to the central (metal) atom. Indeed, the lowest pes bands have been assigned to the metal-carbon σ-bonding orbitals since semi-empirical calculations for tetramethyltin with tetrahedral (T_d) symmetry are in agreement with a highest occupied molecular orbital which is triply degenerate ($3t_2$).

The lowest vertical ionization potentials of three series of homologous tetraalkyltin compounds, viz., R_4Sn, $RSnMe_3$ and R_2SnMe_2, are listed in Table III.(4) For the symmetrical tetraalkyltins, R_4Sn, the values of the first vertical ionization potentials are more or less linearly related to the sums of the Taft polar substituent parameters (σ*) of the alkyl groups, as shown by the straight line which may be drawn through these points. However, considerable scatter is encountered when the same plots of the data are attempted for the two series of the methyl-substituted analogs, viz., $RSnMe_3$ and R_2SnMe_2. In these unsymmetrical tetraalkyltins, symmetry considerations predict the band A of R_4Sn to be split into additional bands. In particular, for the monosubstituted derivatives $RSnMe_3$ with C_{3v} symmetry, band A would be split into an a_1 and doubly degenerate e set, whereas for the disubstituted analogs R_2SnMe_2 with C_{2v} symmetry, it would be split into an a_1, b_1 and b_2 set, as the correlation diagram in Figure 3 illustrates for the complete series of five methylethyl-

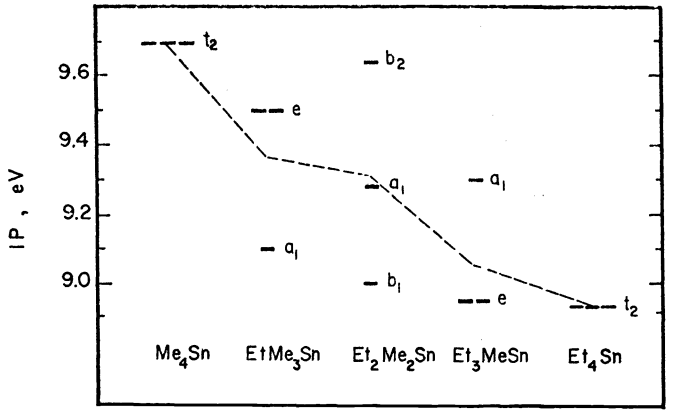

Figure 3. Correlation diagrams for the triply degenerate t_2 molecular orbital of tetramethyltin as a result of successive substitution of ethyl for methyl ligands.

tin compounds. Indeed, the experimental spectrum for Me_3SnBu^t shown in Figure 4a shows a doublet splitting with the expected 1:2 intensity ratio for this low energy band. It is noteworthy that a similar splitting pattern is observed with Et_3SnMe but in a reversed, 2:1

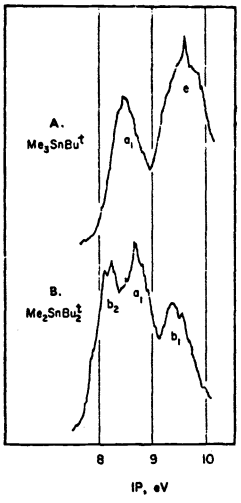

Figure 4. Typical splitting patterns of the lowest energy bands in the photoelectron spectra of unsymmetrical tetraalkyltins: Me_3SnR (upper) and Me_2SnR_2 (lower).

intensity ratio. Furthermore, the pes spectrum of $Me_2SnBu_2^t$ in Figure 4b shows two distinct splittings associated with the three energy levels predicted by this simple formulation.

If we take cognizance of these splittings of the HOMO of tetramethyltin, as they are induced by methyl substitutions, it would appear that the Taft σ* parameter should correlate better with the weighted (center of gravity) average of all the vertical ionization potentials included in the first band **A**. Such an averaging procedure is tantamount to choosing a single (imaginary) ionization potential, $\overline{IP}$, to represent each tetraalkyltin, irrespective of its substitution pattern. [The dashed line in Figure 3 is drawn through $\overline{IP}$ for each $Me_{4-n}Et_nSn$.] Indeed, Figure 5 shows that the averaged ionization potentials for all the various tetraalkyltins are now well correlated with the Taft σ* values by a single line.

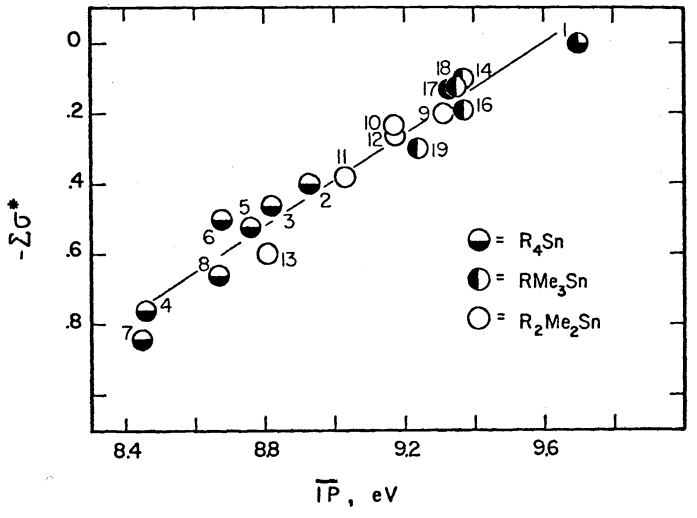

Figure 5. Linear correlation of the weighted average ionization potentials $\overline{IP}$ and Taft Σσ* parameters for the tetraalkyltin compounds listed in Table III.

In the series of monosubstituted tetraalkyltins, $RSnMe_3$, the energy difference Δ between the e and a_1 molecular orbitals (see Figure 3) reflects the perturbation of the triply degenerate t_2 levels in tetramethyltin as a result of successive methyl substitutions at a single methyl ligand [i.e., R = CH_3, CH_3CH_2, $CH_3CH_2CH_2$, $(CH_3)_2CH$, $(CH_3)_3C$, etc.]. As such it is reasonable to expect the magnitude of this splitting to be reflected in the Taft σ* value for R, as shown in Figure 6. It is noteworthy that the linear correlation passes

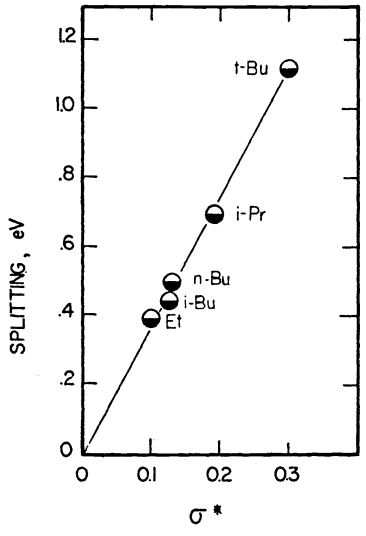

Figure 6. Electronic effects of alkyl ligands (R) measured by Taft σ* values on the splitting of the e and a_1 levels in a series of alkyltrimethyltin $RSnMe_3$ compounds. Note the extrapolation through the origin.

through the origin, i.e.,

$$\Delta = 3.7\sigma^* \text{ eV}$$

in accord with this simple formulation. Thus for a series of unsymmetrical alkyltrimethyltins $RSnMe_3$, the first vertical ionization potential from $HOMO_1$ can be simply related to the ionization potential (IP_1 = 9.70 eV) of tetramethyltin from its Taft σ^* value, i.e.,

$$IP_1(RSnMe_3) = 9.70 - 4.3\,\sigma^*$$

Photoelectron spectroscopy of organometals is also a useful technique with which to compare the donor properties of various types of ligands. Thus, hydrogen can be evaluated as a donor ligand by comparing the ionization potentials of the metal hydrides, SiH_4 (12.36 eV) and GeH_4 (11.98 eV), with those of the methyl analogs, $SiMe_4$ (10.57 eV) and $GeMe_4$ (10.23 eV), or the ethyl analogs, $SiEt_4$ (9.8 eV) and $GeEt_4$ (9.4 eV).(5) It is clear from both series that hydride is a less effective donor than methyl or ethyl ligands. The difference is also clearly shown by an intramolecular comparison in the series of mixed trialkylmetal hydrides R_3MH shown in Figure 7. Here, the two bands $I_D(1)$ and $I_D(2)$ corresponding to

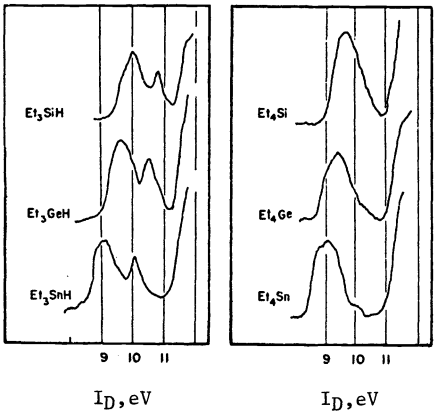

Figure 7. Photoelectron spectra of lowest energy bands for trialkylmetal hydrides (right) and tetraalkylmetals (left).

ionization from the carbon-metal and hydrogen-metal σ-bonding orbitals, respectively, for M = Si, Ge and Sn are all clearly resolved with the expected 2:1 intensity ratios [compare the splitting patterns of the orbitals in Figure 3]. In each case the ionization potential $I_D(1)$ of the molecular orbital associated with the carbon-metal interaction is lower than $I_D(2)$ of the hydrogen-metal interaction, and both follow parallel, increasing trends in the order: Sn < Ge < Si as shown in Figure 8. The same notion derives from the cumulative effects

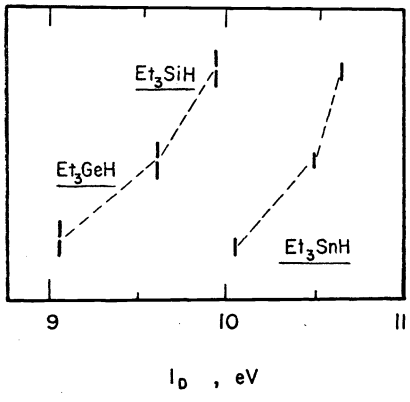

Figure 8. Effect of the metal on $I_D(1)$ [upper energy levels] and $I_D(2)$ [lower energy levels] for trialkylmetal hydrides.

observed in the magnitudes of $I_D(1)$ as well as $I_D(2)$ in proceeding progressively from $GeEt_4$ to GeH_4 through a series of mixed $Et_{4-n}GeH_n$, where n = 1, 2 and 3, as shown by the correlation diagram in Figure 9.

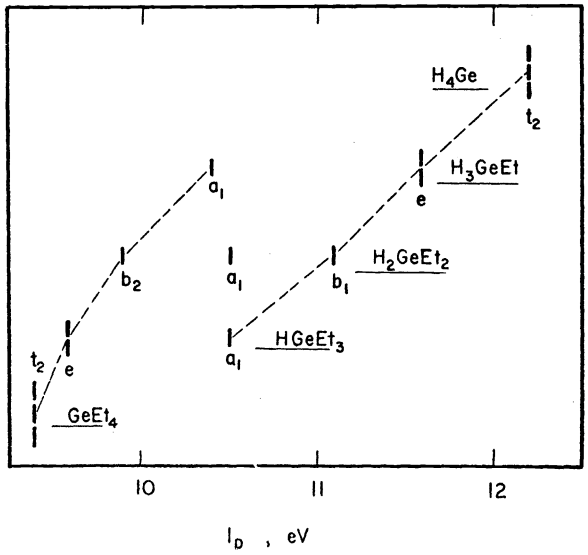

Figure 9. Correlation diagram illustrating the cumulative effects of ethyl ligands on the ionization potentials for $Et_{4-n}GeH_n$.

Alkyl ligands are significantly more effective as donor ligands than halides. For example, the ionization potentials of a series of methylmercury(II) halides(6) are compared in Table IV with the I_D of dimethylmercury, the difference between methyl and chloride being more than 35 kcal mol^{-1}. There is also a marked difference among halides as donor ligands, their effectiveness decreasing in the order: I > Br > Cl in Table IV, in accord with the trend in electron affinities of the halogen atoms [I (3.17 eV), Br (3.36 eV), Cl (3.61 eV)].(7)

Table IV. First Vertical Ionization Potentials (eV) of Binary Mercury(II) Derivatives.

ClHgCl (11.37)	MeHgCl (10.88)	MeHgMe (9.33)
BrHgBr (10.62)	MeHgBr (10.16)	
IHgI (9.50)	MeHgI (9.25)	

The foregoing discussion emphasizes the major role played by ligands in determining the ionization potentials of metal complexes. Indeed, the effect of ligands can overwhelm even the formal oxidation state of the metal. In Table V are listed a series of transition

Table V. Ionization Potentials of Organometals (8)

Organometal	I_D (eV)	Organometal	I_D (eV)
$Mo(CO)_6$	8.4	$Mn(CO)_5CH_3$	8.65
$Mo(CO)_2(dmpe)_2$	6.00	$Mn(CO)_5CF_3$	9.17
$Mo(CO)Cp_2$	5.9	$Mn(CO)_5H$	8.85
MoH_2Cp_2	6.4	$Mn(CO)_3Cp$	8.05
$Mo(CH_3)_2Cp_2$	6.1	$Mn(CO)_5Br$	8.83
		$Mn(CO)_5SnMe_3$	8.63
$Fe(CO)_5$	8.60		
$FeCp_2$	6.88	$Ni(CO)_4$	8.93
$Fe(CO)_2(CH_3)Cp$	7.7	$Ni(PF_3)_4$	8.82
$Fe(CO)_2(Br)Cp$	7.95	$Ni(bipy)Et_2$	6.4
$[Fe(CO)Cp]_4$	6.45	$Ni(allyl)_2$	7.76

metal complexes of molybdenum, manganese, iron and nickel, in which the metal center is present in several formal oxidation states. It is clear that the ionization potentials recorded for each complex bears no direct relationship to the formal oxidation state of the metal. For example, the formal oxidation state of the metal in $Mo(CO)_6$ is Mo(0), yet it has the highest oxidation potential, whereas the Mo(IV) complex $Cp_2Mo(CH_3)_2$ has one of the lowest values, reflecting the donor properties of the cyclopentadienyl and methyl ligands.

III. FACILE CLEAVAGE OF ORGANOMETALLIC RADICAL-IONS

Interest in paramagnetic metal-containing species as described in the foregoing section derives from their behavior as transient intermediates, especially when compared to their diamagnetic counterparts.

Studies with organomercurials and organolead compounds have shown that cleavage of the carbon-metal bond in these compounds occurs readily only after electron transfer. In other words, the radical-ion is much more labile than its diamagnetic precursor, i.e.,

$$R\text{-}m \xrightarrow{-\epsilon} R\text{-}m^{+} \xrightarrow{\text{fast}} R\cdot + m^{+}$$

where m = HgR, PbR_3, SnR_3. Similarly, studies with other organotransition metals show the same results,(9) e.g.,

$$(CH_3CH_2)_2Pt^{II}(PPh_3)_2 \xrightarrow{-\epsilon} (CH_3CH_2)_2Pt^{III}(PPh_3)_2^{+}$$

$$(CH_3CH_2)_2Pt^{III}(PPh_3)_2^{+} \xrightarrow{\text{fast}} CH_3CH_2\cdot + CH_3CH_2Pt^{II}(PPh_3)_2^{+}$$

Other modes of cleavage of the alkyl-metal bonds are also available to radical-ions. For example, organocobalt complexes undergo a facile cationic scission of an alkyl group.(10)

$$R\text{-}Co^{III}(DMG)_2 \xrightarrow{-\epsilon} RCo^{IV}(DMG)_2^{+} \xrightarrow{\text{fast}} \begin{cases} \xrightarrow{H_2O} ROH + Co^{II}(DMG)_2 + H^{+} \\ \xrightarrow{Br^{-}} RBr + Co^{II}(DMG)_2 \end{cases}$$

On the other hand, stable organo-nickel and -gold complexes are known to eliminate dimers rapidly on conversion to the radical-ions:(11)

$$Ph_2Ni^{II}(PEt_3)_2 \xrightarrow{-\epsilon} Ph_2Ni^{III}(PEt_3)_2^{+} \xrightarrow{\text{fast}} Ph\text{-}Ph + Ni^{I}(PEt_3)_2^{+}$$

The diamagnetic, lithium tetramethylaurate(III) and dimethylaurate(I) are thermally quite stable, decomposing at reasonable rates only above 150°C. However, if they are oxidized to the paramagnetic, tetramethylgold(IV) and dimethylgold(II), reductive elimination of ethane is spontaneous, even below 0°C.(12)

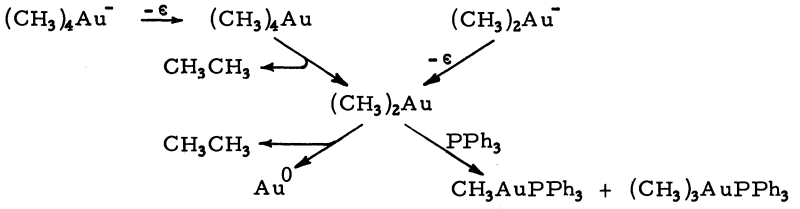

The difference is also shown in the thermal decomposition of the diethyliron(II) complex, $Et_2Fe(bipy)_2$ at 80°C, which affords disproportionation products, but coupling products on oxidation at 0°C,(13)

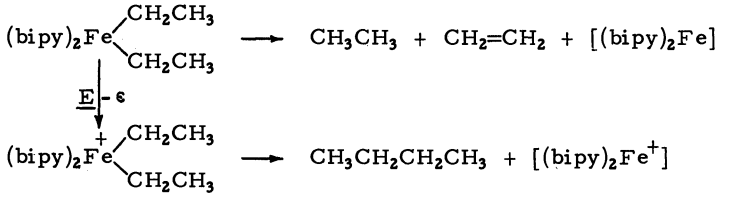

where the oxidant, E = $IrCl_6^{2-}$, Ce(IV), Co(III), Cu(II), Br_2, etc.

No doubt other modes of fragmentation of alkyl-metal bonds will be found as additional organometallic systems are examined.

Facile cleavages of the organometals described above depend on the availability of electron acceptors to effect charge transfer. The efficacy of the acceptor depends to a large degree on its electron affinity. Tetracyanoethylene represents a viable example of an olefinic acceptor, whose electron affinity can be modified by replacement with other substituent groups. Carbon tetrachloride, polyhaloalkanes, halogens and alkyl halides, to a lesser degree, can function as electron acceptors. Molecular oxygen, sulfur dioxide, quinones, ketones, nitroalkanes and arenes, imines, esters and carbonium ions are other examples.(14)

For a given electron acceptor, the charge transfer process will also be facilitated by lowering the ionization potential of the organometal donor. Main group organometals such as dialkylmercury and tetraalkyllead are σ-donors (vide supra), whereas the HOMO in many transition organometals are nonbonding d orbitals. In both types of electron donors, it is worth bearing in mind that the ionization potentials are lower in the anionic species, i.e., the metalate complex, compared to the neutral, uncharged counterpart. Thus, organometal anions are generally among the best electron donors (and nucleophiles) available.(15)

We now wish to focus on the formation of these paramagnetic species by electron transfer and charge transfer processes, using dialkylmercury, tetraalkyltin and -lead compounds as examples.

IV. ELECTRON TRANSFER FROM ORGANOMETALS TO IRON(III) AND IRIDIUM(IV)

Organometals RM are readily cleaved by iron(III) complexes FeL_3^{3+}, where L = 1,10-phenanthroline and related ligands,(16)

$$RM + 2\,FeL_3^{3+} \longrightarrow [R^+] + M^+ + 2\,FeL_3^{2+} \qquad (2)$$

where $[R^+]$ denotes carbonium ion products. The ease of oxidative cleavage of tetraalkyltin by iron(III) complexes is highly dependent on the donor properties of the alkyl groups as measured by the ionization potentials. Thus, in the homologous series of symmetrical tetraalkyltin compounds R_4Sn, the rates progressively increase with α-methyl substitution from R = methyl < ethyl < isopropyl, roughly in the order of $10^0 : 10^4 : 10^7$. This trend, reflecting an inverse steric effect, is counter to any expectation based on a direct bimolecular scission, and it suggests that the activation process does not involve cleavage of the alkyltin bond itself. Instead, electron transfer occurs in a prior, rate-limiting step during oxidative cleavage of organometals. This formulation is in basic accord with the well-established property of tris-phenanthroline and related iron(III) cations to function as oxidants in many inorganic systems. According to the general mechanism presented in Scheme I, the activation process for oxidative cleavage is represented by the electron transfer step 3, which is rapidly followed by homolytic fragmentation of the alkyltin cation-radical [formally an alkyltin(V) species] in eq 4, and further oxidation of the alkyl radical by a second Fe(III) in eq 5.

Scheme I:

$$R_4Sn + Fe^{III} \xrightarrow{k_{et}} R_4Sn^{+\cdot} + Fe^{II} \qquad (3)$$

$$R_4Sn^{+\cdot} \xrightarrow{fast} R_3Sn^+ + R\cdot \qquad (4)$$

$$R\cdot + Fe^{III} \xrightarrow{fast} [R^+] + Fe^{II} \qquad (5)$$

The mechanism in Scheme I accords with all the observations made in this system, including (1) the stoichiometry, energetics and kinetics of the electron transfer step, (2) the observation of alkyl radicals during oxidative cleavage, and (3) the selectivity observed in the oxidative cleavage of methylethyltin compounds. Each of these will be described more fully in the following discussion.

A. Electron Transfer as the Rate-Determining Step

The second-order kinetics for cleavage indicate that alkyltin and only one iron(III) are represented in the rate-determining transition state. The other iron(III) required by the stoichiometry must be involved in a fast subsequent step (vide infra). For an electron transfer process to occur between alkyltin and iron(III), the second-order rate constant k_{et} in eq 3 should reflect the ease of electron detachment from alkyltin, as measured independently by the ionization potential in Table III. Indeed, Figure 10 shows the smooth correlation between the vertical ionization potentials of a series of alkyltin compounds and the log k_{et} for oxidative cleavage. The linearity observed for each of the three oxidants, viz., tris-2,2'-bipyridine, 1,10-phenanthroline and 5-chloro-1,10-phenanthroline iron(III), spans

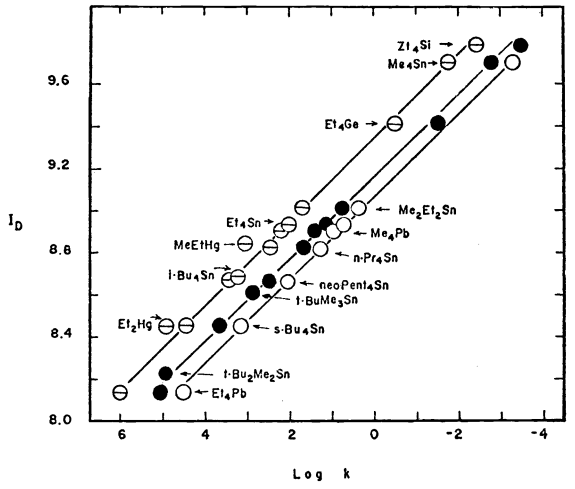

Figure 10. Correlation of the rates (log k) of electron transfer with the ionization potentials I_D for a series of alkylmetals as indicated, using O tris-5-chloro-1,10-phenanthrolineiron(III), O tris-1,10-phenanthroline-iron(III), and O tris-2,2-bipyridineiron(III) as oxidants.

a range of more than 10^8 in rates.

The electron transfer between alkyltin and iron(III) in eq 3 is essentially irreversible since the rate of oxidative cleavage is unaffected by the added iron(II) product. The irreversibility derives in part from the metastable nature of the tetraalkyltin cation-radical (vide infra). Indeed, inability to observe the esr spectrum of the alkyltin cation-radical and the irreversibility of the cyclic voltammetry indicate that its lifetime is very short. Analogous cation-radicals derived from tetraalkyllead, dialkylmercury and dialkylbis(phosphine)-platinum are also unstable.

B. Alkyl Radicals as Prime Intermediates—Oxidation by Iron(III)

The observation of paramagnetic intermediates by spin trapping indicates that alkyl radicals are formed during the oxidative cleavage of alkyltin by iron(III). Furthermore, the scavenging of the alkyl fragments in the presence of molecular oxygen as alkylperoxy products shows that they must depart from tin as the alkyl radicals indicated in eq 4. Accordingly, the isolation of alkyl perchlorates in excellent yields implies that iron(III) is an efficient scavenger of alkyl radicals in eq 5. Indeed, the absence of alkane indicates that hydrogen abstraction from solvent is unable to compete with oxidation,

$$R\cdot \xrightarrow{Fe^{III}} [R^+] + Fe^{II}$$
$$R\cdot \xrightarrow{CH_3CN} RH + \cdot CH_2CN$$

even when oxidative cleavage is carried out with a stoichiometrically limited supply of iron(III), i.e., in the presence of excess alkyltin. Moreover, inability to scavenge all the isopropyl radicals from the oxidative cleavage of $i\text{-PrSnMe}_3$ in the presence of excess oxygen,

$$R\cdot \xrightarrow{Fe^{III}} [R^+] + Fe^{II}$$
$$R\cdot \xrightarrow{O_2} ROO\cdot$$

suggests that the oxidation by iron(III) may approach the diffusion-controlled rates. This conclusion is consistent with the second-order rate constant $k \geq 4 \times 10^8\ M^{-1}\ sec^{-1}$ estimated by Walling and Johnson(17) for the oxidation of hydroxy-methyl radical by Fe_{aq}^{3+} which is a significantly weaker oxidant [E^0 = 0.77 V] than $Fe(phen)_3^{3+}$ [E^0 = 1.22 V] in water.(18) Significantly, the facile oxidations associated with these paramagnetic iron(III) complexes are reminiscent of similar high rates of interaction of alkyl radicals with various copper(II), iridium(IV) and chromium(II) complexes.

C. Selectivity During Fragmentation of Alkyltin Cation-Radicals

Selectivity in the cleavage of alkyl groups from unsymmetrical alkyltin compounds by iron(III) products is represented by the products of cleavage, as illustrated for methylethyltin compounds in eq 6,

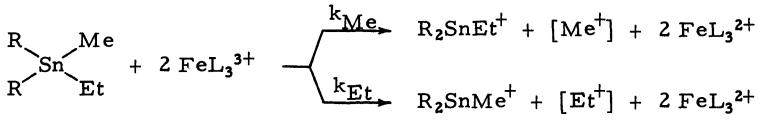

$$R_2Me\text{-}Sn\text{-}R_2Et + 2\,FeL_3^{3+} \xrightarrow{k_{Me}} R_2SnEt^+ + [Me^+] + 2\,FeL_3^{2+}$$
$$\xrightarrow{k_{Et}} R_2SnMe^+ + [Et^+] + 2\,FeL_3^{2+} \qquad (6)$$

where R = Me, Et. The selectivity [S(Et/Me)] represents the ratio of rate constants k_{Et}/k_{Me}.

According to Scheme I, selectivity is established subsequent to the rate-determining electron transfer. During fragmentation of the cation-radical in eq 4, the preference for ethyl cleavage indicated by S(Et/Me) = 27 and 22 for FeL_3^{3+} and $IrCl_6^{2-}$, respectively, in the mixed methylethyltin compounds $Me_{4-n}SnEt_n$, is essentially the same as that observed in the related oxidative cleavage of methylethyllead compounds by $IrCl_6^{2-}$ with S(Et/Me) = 25. Both arise from the fragmentation of the radical-ion:

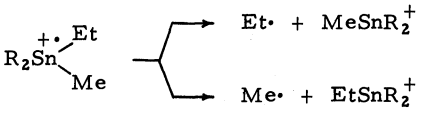

$$R_2Sn^{+\cdot}(Et)(Me) \longrightarrow Et\cdot + MeSnR_2^+$$
$$\longrightarrow Me\cdot + EtSnR_2^+ \qquad (7)$$

Similar selectivities are observed in the mass spectral cracking patterns of methylethyltin compounds although reduced in magnitude. The latter doubtlessly reflects the loss in selectivity of highly energetic species formed by electron impact relative to those cation-radicals formed in solution. The effect of solvation cannot be assessed quantitatively, but the qualitative trends in selectivity, both in solution and in the gas phase, are unmistakable. The prevailing factor which determines the predominance of ethyl over methyl cleavage is the strengths of the relevant alkyl-metal bonds. These values can be evaluated from the mean bond energies for Et_4Sn and Me_4Sn which are 46 and 54 kcal mol^{-1}, respectively, and for Et_4Pb and Me_4Pb which are 33 and 40 kcal mol^{-1}, respectively.(1)

It is noteworthy that all of these unimolecular selectivities are inverted relative to those observed in other bimolecular processes. For example, the electrophilic cleavage of methylethyllead compounds by acid [S(Et/Me) = 0.11 and 0.021 for HOAc and H_2OAc^+, respectively] and metal ions [S(Et/Me) = 0.018 and 0.022 for CuOAc and $CuCl_2$, respectively] all involve the direct scission of the alkyl-metal bond by the electrophile.(19) As such, the inverted order in selectivity in each of these processes (i.e., methyl cleaved in preference to ethyl) reflects the dominance of steric constraints over electronic effects in bimolecular transition states.

Indeed, differences in selectivity patterns provide one of the best diagnostic methods for distinguishing electrophilic (two-equivalent) from electron transfer (one-equivalent) mechanisms for the cleavage of alkylmetals. More relevant to the issue here, the similar selectivities [clustering around S(Et/Me) = 25] observed for the oxidative cleavage of methylethyltin compounds induced by FeL_3^{3+} and by $IrCl_6^{2-}$ are only consistent with the cation-radical as the common intermediate leading directly to cleavage, as described in eq 7. It is conceivable that the cation-radical $R_4Sn^{+\cdot}$ formed in eq 3 is not free, and the degree to which it is still associated with the reduced iron(II) species would affect its subsequent reactivity. In order to evaluate this problem, let us consider whether the electron transfer step itself conforms to the Marcus criterion for an outer-sphere mechanism. We next compare the oxidation of an alkylmetal RM by iron(III) with that effected by hexachloroiridate(IV),

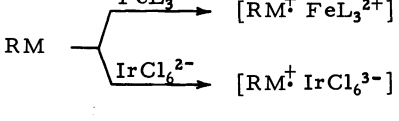

$$RM \xrightarrow{FeL_3^{3+}} [RM^{+\cdot}\ FeL_3^{2+}]$$
$$\xrightarrow{IrCl_6^{2-}} [RM^{+\cdot}\ IrCl_6^{3-}]$$

Such a comparison also focusses on the ion-pairing energies, since the electrostatic potential in the ion pair derived from iron(III) is repulsive, whereas it clearly changes to an attractive energy in the ion pair derived from iridate(IV).

D. Outer-Sphere Processes for Electron Transfer from Alkylmetals to Iron(III) Complexes

In the outer-sphere reaction of alkylmetals with iron(III), Marcus theory predicts a slope of 0.5 in the correlation of the rates of electron transfer (log k) with the difference in standard free energy changes of RM and FeL_3^{3+}.

(1) Structural effects of iron(III). For a particular alkylmetal, log k for electron transfer is linear with the standard oxidation potential of the iron(III) complexes. The slope

of the correlation in eq 8,

$$\log k = 8.75\ E^0 + \text{constant} \qquad (8)$$

is equivalent to that of a linear free energy plot with $\Delta G^{\ddagger} = 0.50\ \Delta G^0 + \text{constant}$, predicted by the Marcus theory for outer-sphere electron transfer. It is noteworthy that the family of lines in Figure 11 for all eleven alkylmetals pass through the experimental points with

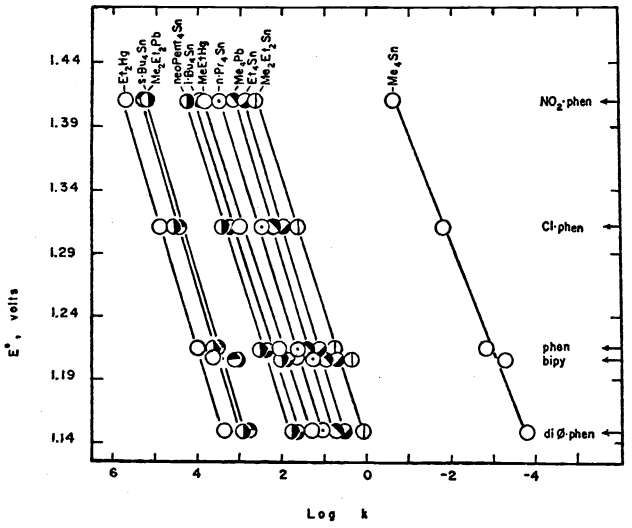

Figure 11. The Marcus plot of standard electrode potentials (E^0 vs. SHE) for various iron(III) complexes with the second-order rate constant (log k) for electron transfer from the alkylmetals listed at the top.

slopes [8.9±0.4] close to this value. Both two-coordinate dialkylmercury compounds and four-coordinate tetraalkyltin as well as -lead compounds are generally included in this correlation. Furthermore, the points for the iron(III) complex with the most sterically hindered ligand, L = 4,7-diphenyl-1,10-phenanthroline, also fall close to the lines. If the alkylmetal must penetrate the octahedral, tris ligand sphere around iron(III) before electron transfer can take place, the substantial difference in steric effects between 4,7-diphenylphenanthroline and 1,10-phenanthroline should be manifested most either with the linear mercury alkyls or with the highly congested tetraneopentyltin. Thus, the linear relationships generally observed suggest a transition state in which the alkylmetal is located along the periphery of the iron(III) complex. Electron transfer probably could occur via the π-orbitals of the phenanthroline ligand. Indeed, the negative deviations consistently observed with the analogous bipyridine iron(III) complex in Figure 11 accord with the less extensive π-conjugation in this ligand.

(2) Structural effects of the alkylmetal—HOMO and steric effects. For a particular iron(III) complex, log k for electron transfer is also linear with the ionization potential of the alkylmetal. The smooth correlation in Figure 10 includes the tetraalkylmetals of silicon, germanium, tin and lead as well as the two-coordinate dialkylmercury compounds. The linearity spans a range of almost 10^8 in the rates of electron transfer. Furthermore, the correlation,

$$\log k = -4.9\ I_D + \text{constant} \qquad (9)$$

accords with the known relationship between I_D and E^0 and provides additional support for the outer-sphere mechanism.

If only tetraalkyltin and -lead compounds are considered, the linear correlation in Figure 10 is excellent. It suggests that the solvation terms are essentially constant throughout the series of tin and lead compounds. This is not unreasonable since the effective size of the cation-radical from lead(V) is probably not much larger than that of tin(V) due to the lanthanide contraction. However, the most important feature of the correlation in Figure 10 is the striking absence of steric effects with changes in the structures of the alkyl ligands. In particular, increasing the branching of the alkyl ligand at the β-carbon with methyl groups in the homologous series: CH_3CH_2, CH_3CH_2CH, $(CH_3)_2CHCH_2$ and $(CH_3)_3CCH_2$, leads to no deviation from the linear free energy correlation. Even the oxidative cleavage of the sterically hindered tetra-neopentyl is included precisely in the correlations with all three iron(III) complexes. The same applies to α-branching in the series:

CH_3, CH_3CH_2, $(CH_3)_2CH$ and $(CH_3)_3C$.

E. Inner-Sphere Processes for Electron Transfer from Alkylmetals to Hexachloroiridate(IV)

Alkylmetals are oxidatively cleaved by hexachloroiridate(IV) by essentially the same mechanism as that described in Scheme I for iron(III). For example, the facile reaction with the homoleptic alkylmetals of mercury and lead has been shown to proceed via a rate-limiting electron transfer.

$$RM + IrCl_6^{2-} \xrightarrow{k} RM^{+\cdot} + IrCl_6^{2-} \qquad (10)$$

The products, stoichiometry, and kinetics indicate that the tin derivatives in this study also react by the same mechanism, as shown below:

Scheme II:

$$R_4Sn + IrCl_6^{2-} \xrightarrow{k_{et}} R_4Sn^{+\cdot} + IrCl_6^{3-} \qquad (11)$$

$$R_4Sn^{+} \xrightarrow{fast} R_3Sn^{+\cdot} + R\cdot \qquad (12)$$

$$R\cdot + IrCl_6^{2-} \xrightarrow{fast} RCl + IrCl_5^{2-} \qquad (13)$$

The reduction potential of hexachloroiridate(IV) in acetonitrile solution is 0.67 volts, which is less than the E^0 of the iron(III) complexes. However, the second-order rate constants for electron transfer from both tetramethyltin and -lead to hexachloroiridate(IV) are significantly larger than those predicted from an extrapolation of the correlations in Figure 11. Indeed, tetramethyltin reacts about 10^7 times faster than expected. Thus in contrast to iron(III), an inner-sphere contribution to electron transfer is indicated in the case of hexachloroiridate(IV), and it suggests that the alkylmetal can be approached by hexachloroiridate(IV) closer than by iron(III) in the transition state for electron transfer. In other words, steric effects are more important in electron transfer reactions with hexachloroiridate(IV) than those with iron(III). Indeed, the smooth correlation shown in Figure 10 between I_D and log k_{et} for outer-sphere electron transfer with iron(III) is no longer valid. Instead, the rates of oxidative cleavage of the same alkylmetals by hexachloroiridate(IV) are depicted in Figure 12. However, despite the random, "buckshot" appearance of the plot, a closer

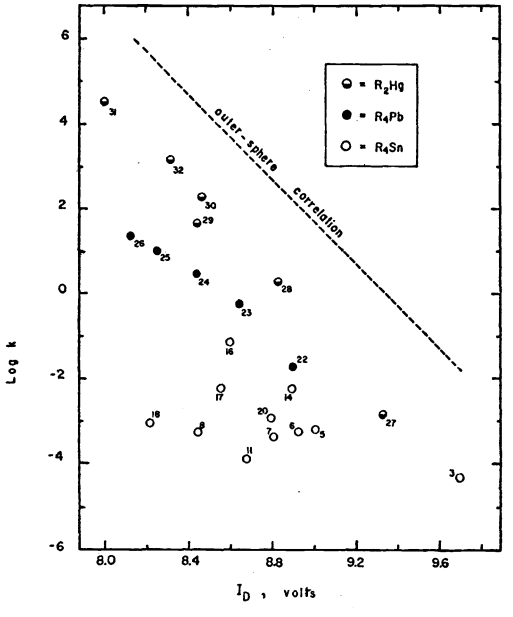

Figure 12. The relationship between the rates of electron transfer (log k) to hexachloroiridate(IV) and the ionization potentials I_D of a series of tetraalkyltin compounds indicated by open circles O. Comparison with ● methylethyllead and ⊖ dialkylmercury compounds. The numbers refer to compounds designated in Table VI. The outer-sphere slope is indicated by the dashed line taken from Figure 10 for tris-5-chloro-1,10-phenanthrolineiron(III).

scrutiny of the data shows a systematic trend among a limited number of related compounds. For purposes of calibration, the dashed line in Figure 12 is the correlation with iron(III), in which the slope is representative of outer-sphere electron transfer from these alkylmetals (vide supra). The correlations of hexachloroiridate(IV) with the methylethyl derivatives of both mercury and lead are fairly linear, with approximately this slope, but not on the same line. Apparently with these less hindered alkylmetals, the rates of electron transfer to hexachloroiridate(IV) are determined more by electronic effects (i.e., the HOMOs described in Figure 5) rather than by steric effects. A greater variety of alkyl structures are included among the tetraalkyltin derivatives and the points in Figure 12 show considerable, but accountable scatter. Thus, the negative deviation from the outer-sphere slope is most pronounced with the α- and β-branched alkyl groups, i.e., the isopropyl, isobutyl and t-butyl derivatives. Clearly the hindered alkyltin compounds are cleaved by hexachloroiridate(IV) much more slowly than their values of I_D alone would indicate. A similar conclusion may be reached from the varying magnitudes of Δlog k for different alkylmetals. Such a steric effect must reflect the perturbation of the inner sphere of the alkylmetal in the transition state for electron transfer. Indeed, this conclusion can be used as an operational criterion for an inner-sphere mechanism of electron transfer from alkylmetals to hexachloroiridate(IV).

F. A Continuum of Outer- and Inner-Sphere Processes for Electron Transfer from Alkylmetals

The concepts of outer-sphere and inner-sphere electron transfer as we have employed here depend on the availability of various alkyl groups as highly "tunable" probes for steric effects. As such, we might ask how these processes basically differ since the alkylmetal cation-radical is an intermediate which is common to both iron(III) and iridate(IV). Thus, selectivity studies demonstrate that there is no direct, covalent bond formed between the alkylmetal and hexachloroiridate(IV) during inner-sphere electron transfer. Outer- and inner-sphere processes with alkylmetals may be distinguished by the magnitudes of the intermolecular separation between the alkylmetal and the oxidant in the transition states for electron transfer. The driving force as well as electrostatic forces are expected to contribute to the "tightness" of these transition states. In the inner-sphere activated complex, changes in the steric properties of alkyl ligands indicate that the alkylmetal is geometrically perturbed, and we tentatively suggest that a precursor complex is formed in which the tetraalkyltin achieves a quasi five-coordinate configuration reminiscent of a variety of trigonal bipyramidal structures known for tin(IV) derivatives. According to this proposal, substitution-inert organometals can undergo outer-sphere as well as inner-sphere electron transfer. For tetraalkylmetals the inner-sphere process is subject to steric hindrance by the alkyl groups which may be relieved by partial distortion of the configuration at the metal center. This formulation implies that a continuum of outer-sphere and inner-sphere processes is possible for electron transfer which differ principally in geometrical constraints. This problem is discussed further in the next section, in which the same organometals are subjected to charge transfer interactions.

V. CHARGE TRANSFER PROCESSES OF ORGANOMETALS WITH TETRACYANOETHYLENE

Another manifestation of the properties of electron donors is their ability to form charge-transfer complexes. Thus, the addition of dialkylmercury to a solution of tetracyanoethylene (TCNE) results in weak but distinct colors characteristic of the mercurial added. The stability of the band also varies, being the most stable with dimethylmercury. The transient bands from diisopropyl and di-tert-butylmercury were recorded at -77°C, but even at this temperature the solutions bleach rapidly as the charge transfer (CT) complexes undergo further thermal reactions leading to the insertion of TCNE into a single alkylmercury bond.(20)

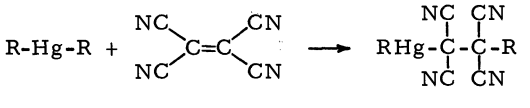

(14)

A similar series of observations are also made with tetraalkyltin compounds for which the formation of the charge transfer complex is:

$$R_4Sn + TCNE \underset{}{\overset{K_{CT}}{\rightleftharpoons}} [R_4Sn\ TCNE] \qquad (15)$$

The bands are broad, as is characteristic of intermolecular charge transfer spectra, and the absorption maxima are highly dependent on the structure of the tetraalkyltin compounds listed in Table VI.(21)

According to the valence-bond description, the frequency of the CT band corresponds roughly to the energy required to transfer an electron from R_2Hg to TCNE. [In the following, R_2Hg and R_4Sn are used interchangeably to denote the reactions of organometals RM generally.]

Table VI. The Formation and Reaction of Charge Transfer Complexes of Alkyltin and Tetracyanoethylene.[a]

No.	Alkyltin	I_D (eV)	ν_{CT} (10^{-4} cm^{-1})	ϵ_{CT} (M^{-1} cm^{-1})	log K_{CT} (M^{-1})	log k_T (M^{-1} sec^{-1})
1	Me_4Sn	9.69	2.90	500	-0.76	-4.82
2	Et_4Sn	8.90	2.38	167	-0.28	-3.07
3	n-Pr_4Sn	8.82	2.41	29	0.34	-2.59
4	n-Bu_4Sn	8.76	2.40	16	0.89	-2.04
5	$EtMe_3Sn$		2.68	222	-0.61	-4.04
6	n-$PrMe_3Sn$	9.1	2.78	200	-0.61	-4.70
7	n-$BuMe_3Sn$	-	2.84	172	-0.68	-4.54
8	Et_2Me_2Sn	9.01	2.62	143	-0.10	-3.34
9	n-Pr_2Me_2Sn	8.8	2.58	77	0.16	-3.37
10	n-Bu_2Me_2Sn	8.8	2.59	50	0.04	-3.20
11	i-Pr_4Sn	8.46	2.29	95	0.0	-2.85
12	s-Bu_4Sn	8.45	2.33	71	0.39	-2.21
13	i-Bu_4Sn	8.68	2.41	125	-0.52	-3.66
14	i-$PrMe_3Sn$	8.9	2.47	40	0.0	-3.19
15	t-$BuMe_3Sn$	8.6	2.35	-	-	-2.18
16	i-Pr_2Me_2Sn	8.56	2.38	118	-0.02	-2.92
17	t-Bu_2Me_2Sn	8.22	2.38	77	-0.19	-3.43
18	i-Bu_2Et_2Sn		2.38	143	-0.40	-3.48
19	neo-$Pent_3EtSn$			-	-	-4.14
20	neo-$Pent_4Sn$	8.67	-	-		<-6

[a] Charge transfer spectra measured in chloroform solution. Second-order rate constants measured in acetonitrile at 25°C.

$$[R_2Hg\ TCNE] \xrightarrow{h\nu_{CT}} [R_2Hg^{+\cdot}\ TCNE^{-\cdot}] \tag{16}$$

For weakly associating systems, such as these are, $h\nu_{CT}$ is approximated by eq 17,

$$h\nu_{CT} = I_D - E_A - [G_1 - G_0] \tag{17}$$

where I_D and E_A refer to the vertical ionization potential of R_2Hg and the electron affinity of TCNE, respectively, and G_1, the dominant term in the brackets, involves Coulombic interaction in the excited state. With TCNE as the common acceptor, Figure 13 shows the linear relationship between $h\nu_{CT}$ and the vertical ionization potential for the series of R_2Hg.

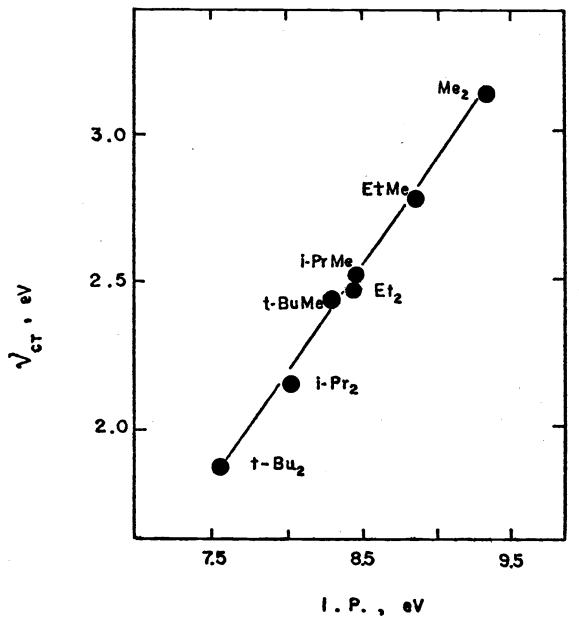

Figure 13. Correlation of the ionization potentials of dialkylmercury compounds with the frequency of the charge transfer band with TCNE.

The interaction of an electron donor with an electron acceptor may lead to a variety of thermal processes including electron transfer, covalent bond formation, etc. For the weak donor-acceptor interactions pertaining to the dialkylmercury-TCNE systems, we use the representation in eqs 18-20, in which insertion occurs subsequent to electron transfer.

Scheme III:

$$R_2Hg + TCNE \rightleftharpoons [R_2Hg\ ,\ TCNE] \tag{18}$$

$$[R_2Hg\ ,\ TCNE] \xrightarrow{k} [R_2Hg^{\ddagger\bullet}\ TCNE^{-\bullet}] \tag{19}$$

$$[R_2Hg^{\ddagger\bullet}\ ,\ TCNE] \xrightarrow{fast} RHg\text{-}TCNE\text{-}R \tag{20}$$

The relationship between the rate (i.e., log k) of the thermal process leading to insertion and the energy of the charge transfer transition in the donor-acceptor complex is illustrated by the potential energy curves below:

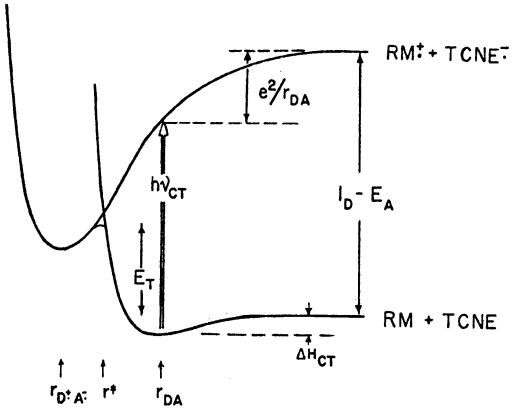

Figure 14. The relationship between thermal (E_T) and photochemical ($h\nu_{CT}$) activation of electron transfer proceeding from the charge transfer complex.

It can be seen from this formulation that the optical transition energy $h\nu_{CT}$ and the thermal activation energy E_T both depend on the potential energy of the ion pair. Lowering the ionization potential of the donor will cause a red shift in the charge transfer band and also lead to an increase in the rate of the thermal reaction. Indeed, there exists a linear correlation between log k for insertion and the frequency of the charge transfer band of a series of dialkylmercury compounds $RHgCH_3$ with TCNE, i.e., $\log k = \alpha\, \nu_{CT}$, where α is the proportionality constant. According to this mechanism, the actual transfer of an alkyl group from dialkylmercury to TCNE occurs in eq 20, subsequent to the rate-limiting electron transfer step in eq 19. The rapid alkylation of TCNE involves the transfer of an alkyl group from $R_2Hg^{\ddagger\bullet}$ which is metastable (vide infra).

A. The Mechanism of Insertion—Thermal and Photochemical Processes

The observation of the charge transfer complex of alkyltin and TCNE does not, by itself, prove that the complex lies along the reaction pathway to insertion. Complex formation may represent an unrelated side reaction. The difference lies in whether the rate-limiting, second-order rate constant k_T for electron transfer is a product, $K_{CT}k_{et}$, as represented in eqs 21 and 22,

$$R_4Sn + TCNE \overset{K_{CT}}{\rightleftharpoons} [R_4Sn\ TCNE] \tag{21}$$

$$[R_4Sn\ TCNE] \xrightarrow{k_{et}} [R_4Sn^{\ddagger\bullet}\ TCNE^{-\bullet}] \tag{22}$$

or a simple bimolecular constant representing the direct reaction of alkyltin and TCNE, distinct from the charge transfer complex as in eq 23.

$$[R_4Sn\ TCNE] \overset{K_{CT}}{\rightleftharpoons} R_4Sn + TCNE \xrightarrow{k_{et}} R_4Sn^{\ddagger\bullet} + TCNE^{-\bullet} \tag{23}$$

The reasons for favoring electron transfer to proceed directly from the alkyltin-TCNE complex derive from (1) the correlation of the formation constant K_{CT} with the phenomenological rate constant k_T, as well as the intimate relationship between (2) the photochemical activation and (3) the thermal activation of electron transfer. Following a discussion of these mechanistic points, we wish to consider (4) the nature and fate of the ion pair as an intermediate common to both thermal and photochemical activation and (5) steric effects involved in the electron transfer within the charge transfer complex.

B. Correlation of K_{CT} and k_T for the Thermal Insertion Reaction

The measured second-order rate constant k_T for the reaction of alkyltin and TCNE is plotted against the formation constant K_{CT} for the charge transfer complex in Figure 15.

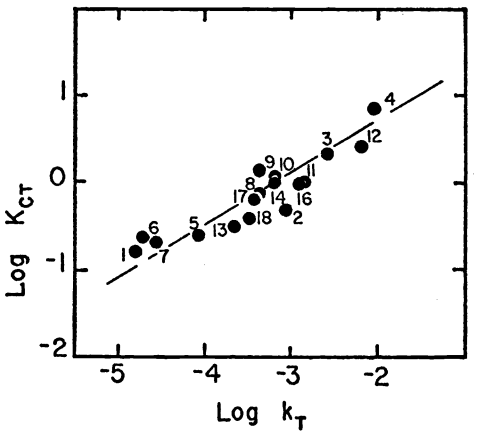

Figure 15. The parallel between formation constants of charge transfer complexes and the thermal rates of insertion. Numbers refer to tetraalkyltin compounds in Table VI.

Despite the absence of any correlation of K_{CT} with the ionization potential I_D of tetraalkyltin or the frequency ν_{CT} of the charge transfer complex due to steric effects as discussed above, there is a reasonable correlation with the overall second-order rate constant. Such a parallel relationship between K_{CT} and k_T is more in keeping with the charge transfer complex as an intermediate, rather than as an unrelated side product.

C. Photochemical Activation of Insertion

Photoinsertion, resulting from irradiation directly at 436 nm or at 546 nm, where only the charge transfer absorption occurs, must necessarily proceed via excitation of the charge transfer complex and not that of either alkyltin or TCNE alone.

$$[R_4Sn\ TCNE] \xrightarrow{h\nu_{CT}} [R_4Sn^{+\cdot}\ TCNE^{-\cdot}] \qquad (24)$$

Moreover, esr studies demonstrate that alkyl radicals and TCNE anion-radicals are intermediates formed simultaneously during this photoactivation. They must result from a dark reaction following electron transfer, i.e.,

$$[R_4Sn^{+\cdot}\ TCNE^{-\cdot}] \xrightarrow{fast} [R\cdot\ R_3Sn^{+}\ TCNE^{-\cdot}] \qquad (25)$$

in accord with the known instability of the tetraalkyltin cation-radical. The lifetime of the pair of caged radicals in eq 25 is exceedingly short, and their direct esr observation is only allowed by the physical constraints imposed by the frozen matrix. Radicals produced during charge transfer excitation must be intermediates in photoinsertion since the quantum yield of 0.2, measured as a lower limit for radical production in a frozen matrix at -175°C, is still rather large and approaches the quantum yield of one, measured in solution for the photoinsertion process itself. These observations are readily accounted for by the sequence of steps described in eqs 21 and 22. Photoinsertion must then follow directly from the cage collapse of these fragments formed in eq 25, i.e.,

$$[R\cdot\ R_3Sn^{+}\ TCNE^{-\cdot}] \xrightarrow{fast} [R_3Sn\text{-}TCNE\text{-}R] \qquad (26)$$

The mechanism of photoinsertion is thus represented by the sequence of reactions given by eqs 21, 22, 25 and 26.

D. Thermal Activation of Insertion

The observed second-order kinetics indicates that both alkylmetal and TCNE are present in the rate-limiting step for insertion. The importance of electron transfer in the transition state is reflected in the parallel relationship between the thermal rates of insertion and the energetics of electron detachment measured independently by the ionization potentials.

The potential energy diagrams in Figure 14 illustrate how photoactivation via the charge transfer transition $h\nu_{CT}$ is related to the thermal activation, designated as E_T. Indeed, among a limited series of methylethyllead compounds with similar steric properties, there is a reasonable linear relationship between $h\nu_{CT}$ and log k_T for photochemical and thermal insertion, respectively. A similar general trend in this correlation also pertains to the alkyltin analogs examined here. This correlation, coupled with the relationship observed between log k_T and the K_{CT}, leads to the conclusion that electron transfer proceeds from the same charge transfer complex,

$$[R_4Sn\ TCNE] \longrightarrow [R_4Sn^{+\cdot}\ TCNE^{-\cdot}] \qquad (27)$$

which was proven to be directly involved in photochemical activation. The subsequent reactions leading to insertion are the same as the rapid dark reactions in eqs 25 and 26 presented for the photoinduced insertion. Accordingly, thermal and photoactivation of insertion share common mechanistic pathways. Any difference may lie in the nature of the paramagnetic ion pair resulting from electron transfer within the charge transfer complex as represented in eqs 24 and 27.

E. Ion Pairs as Common Intermediates in Thermal and Photochemical Insertion

The Franck-Condon limitations placed on the photoinduced electron transfer in eq 24 restrict the intermolecular separation in the excited ion pair to that of the charge transfer complex. In the thermal process, the same or a similar ion pair is also an intermediate derived by electron transfer in eq 27. Since these paramagnetic ion pairs are formed subsequent to the rate-determining step, their properties are best examined either by direct spectroscopic examination or by product selectivity.

Attempts to observe the triplet esr spectrum of the ion pair, produced either thermally or photochemically in solution or in a frozen matrix, were all consistently unsuccessful. The negative results of the CIDNP studies also point out that the $R_4Sn^{+\cdot}$ moiety is very short-lived. The direct comparison between the thermally and the photochemically induced formation of the ion pair, however, can be made by examining the selectivity in the fragmentation patterns of the alkyltin moiety prior to insertion. For example, the insertion into either the Me-Sn or the Et-Sn bond in the series of methylethyltin compounds is governed by the scission of the relevant bond in the paramagnetic alkyltin moiety represented above in eq 7. The extent to which fragmentation of this cation-radical proceeds from an excited state or from a geometrically distorted configuration or is influenced by $TCNE^{-\cdot}$, its counterion within the cage, would be reflected in changes in ethyl/methyl selectivity for insertion. The striking similarities of S(Et/Me) for both the thermal and photochemical processes strongly suggest that insertion proceeds from more or less the same paramagnetic ion pair. It is noteworthy that this selectivity is reasonably close to that (~6) observed in the unimolecular fragmentation of the molecule ion generated upon electron impact in the gas phase.

The observation of stable TCNE radicals in solution, either as $TCNE^{-\cdot}$ and $R_3SnTCNE^{\cdot}$, arises by a side reaction. Integration of the esr signal indicates that these species generally constitute <0.1% of the reaction. However, measurement of the esr linewidth dependence of TCNE radicals as a function of TCNE concentration indicates that they can undergo exchange at rates of $3 \times 10^9\ M^{-1}\ sec^{-1}$. Similar exchanges lead to broadening of the nmr lines in the absence of an acetic acid quench. According to the Scheme presented in eqs 25 and 26, these radicals arise from partial diffusive separation from the cage, i.e.,

$$[R^{\cdot}\ R_3Sn^{+}\ TCNE^{-\cdot}] \xrightarrow{\text{diffuse}} R_3SnTCNE^{\cdot} + R^{\cdot}\ ,\ \text{etc.} \qquad (28)$$

Unfortunately, our attempts to observe CIDNP effects associated with such a competition have been unsuccessful as yet.

F. Steric Effects in Electron Transfer from Charge Transfer Complexes

If the ion pairs described in the preceding section resulted from simple electron transfer between alkyltin and TCNE, it is expected that the rates (log k_T) would correlate linearly with the ionization potentials of the alkyltin compounds. Indeed, such a linear correlation can be observed in Figure 16 for the insertion reaction with a limited series of methylethyllead compounds with similar steric properties. If the correlation is extended to the greater variety of alkyltin structures available in this study, it shows the same general trend, but with considerable scatter. However, a closer examination of the data reveals that deviations are systematic and most marked with sterically hindered compounds,

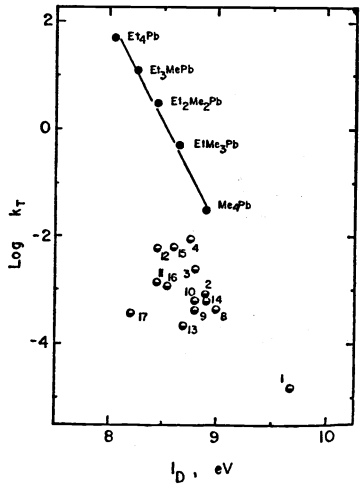

Figure 16. Steric effects in the correlation of the thermal rates of insertion and the ionization potentials of tetraalkyltin designated by numbers in Table VI. Comparison with methylethyllead compounds.

increasing roughly in the order: t-Bu > i-Bu > i-Pr > Et >> Me. Tetra-neopentyltin, the most sterically hindered compound, does not react at all.

The same general steric effects are shown in the correlation of log k_T with the charge transfer frequency ν_{CT} and lends further support to the charge transfer complex as an intermediate in both thermal and photochemical insertions. The intermolecular distance between R_4Sn and TCNE in the transition state for electron transfer must be sufficiently small to allow for these variations. Indeed, a comparison with the inner-sphere pathway for electron transfer between the same alkyltin compounds and hexachloroiridate(IV) suggests that TCNE may have penetrated the coordination sphere of alkyltin sufficiently to cause significant distortion of the tetrahedral tin structure.

VI. QUANTITATIVE EVALUATION OF STERIC EFFECTS IN ELECTRON TRANSFER AND CHARGE TRANSFER

For TCNE interacting with a series of related alkylmetals, it follows from eq 17 that the difference in the electrostatic terms ΔE between a particular alkylmetal RM relative to a chosen reference RM_0 is:(22)

$$\Delta E = \Delta I_D - \Delta h\nu_{CT} \tag{29}$$

where ΔI_D is the difference in the ionization potentials between RM and RM_0 and $\Delta h\nu_{CT}$ is the difference in their charge transfer energies. The conversion of this energy difference to a rate factor $\Delta \log k$ is given by eq 30.

$$\Delta E = 2.3\ RT\ \Delta \log k \tag{30}$$

[At this juncture, it is convenient to consider the rate factor $\Delta \log k$ simply as a contribution of steric effects to the rate of electron transfer.] A corrected value of the electron transfer rate constant log k^{corr}_{TCNE} may be expressed as:

$$\log k^{corr}_{TCNE} = \log k_{TCNE} + \Delta \log k \tag{31}$$

where k_{TCNE} is the experimental second-order rate constant. Under these circumstances, log k^{corr}_{TCNE} represents the electron transfer rate constant under hypothetical conditions of constant steric effects (i.e., relative to that of the chosen standard $RM_0 = Me_4Sn$). Stated alternatively, log k^{corr}_{TCNE}, or its equivalent $\Delta G^{\ddagger}_{corr}$, is the form to be related to the driving force of the electron transfer (ΔG^0), in the absence of steric effects. Figure 17 shows the new correlation of the data previously presented in Figure 16 for the electron transfer rate constants between TCNE and a series of tetraalkyltin compounds. The dashed line in Figure 17 is arbitrarily drawn with a Brönsted slope of $\alpha = 1$ through the point for Me_4Sn.

Let us assume for the moment that steric effects in electron transfer from tetraalkyltin to hexachloroiridate is also the same as those to tetracyanoethylene. Then, the electron transfer rate constant log k_{Ir} can be corrected by an amount $\Delta \log k$ to afford log k^{corr}_{Ir} in a

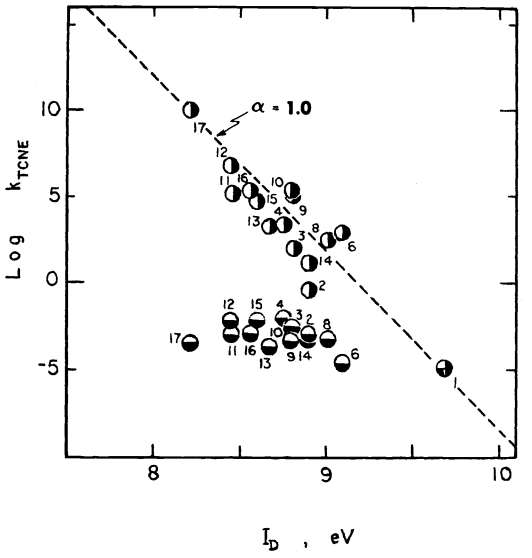

Figure 17. The linear free energy relationship of the electron transfer rate constant for tetraalkyltin and TCNE: ◒ before and ◑ after correction for steric effects.

manner similar to eq 31. The linear free energy plot is presented in Figure 18, with the dashed line showing the correlation of k_{Ir}^{corr} with a Brönsted slope of α = 1.

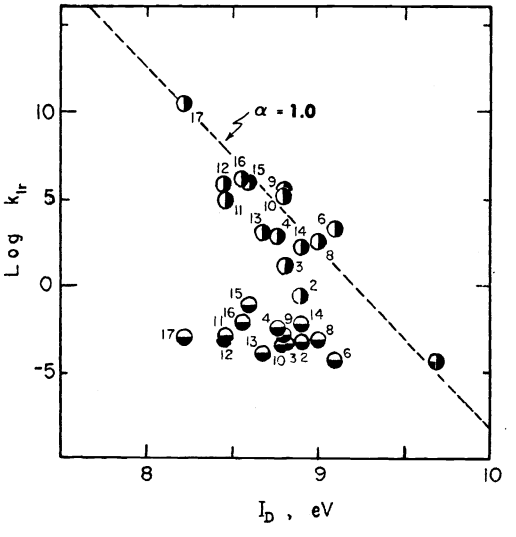

Figure 18. The linear free energy relationship of the electron transfer rate constant for tetraalkyltin and $IrCl_6^{2-}$: ◒ before and ◑ after correction for steric effects.

It is striking that a single linear free energy relationship, i.e.,

$$\log k = -9.8\, I_D + \text{constant} \tag{32}$$

can be obtained empirically by using a simple correction, $\Delta \log k$ from eq 30, to correlate the rates of electron transfer to both TCNE and $IrCl_6^{2-}$ from a wide variety of the organometals R_4Sn, R_4Pb and R_2Hg containing alkyl ligands with diverse steric and polar parameters.

Equation 32 is equivalent to the free energy changes expressed more familiarly as:

$$\Delta G^{\ddagger} = 1.0\, \Delta G^{0} + \text{constant} \tag{33}$$

The coefficient 1.0 in eq 33 is the Brönsted coefficient α, and it differs from $\alpha = 0.5$ for outer-sphere electron transfer found for FeL_3^{3+}, as described above.

It is important to emphasize that the derivation of the linear free energy relationship in eq 32, or its equivalent in eq 33, obtains directly from the experimental data by a purely operational approach with no extensive assumptions. We now proceed to its possible implications, especially as it may relate to the inner-sphere mechanism for electron transfer.

In the region of weak overlap as in outer-sphere mechanisms, the Marcus eq 8 provides a theoretical basis for electron transfer rates, as shown for alkylmetals and FeL_3^{3+}. When electron transfer involves considerable resonance splitting as in a variety of inner-sphere mechanisms, eq 8 no longer applies, and the situation is not well provided by theory. At one extreme of an inner-sphere mechanism, where $\Delta G^0 \geq \lambda$ (i.e., endergonic processes), Marcus predicted the relationship:(23)

$$\Delta G^{\ddagger} = \Delta G^0 + w^p \tag{34}$$

where w^p is the work term required to bring the products to within a mean separation $r^{\ddagger}$ in the activated complex. Equation 34 corresponds to a linear free energy relationship with the Brönsted slope $\alpha = 1$. Since the microscopic reverse represents a diffusion-controlled electron transfer, in qualitative terms eq 33 can be related to the Hammond postulate for endothermic processes.

In order to evaluate the work terms for various alkylmetals in eq 34, values of the free energy change ΔG^0 are required. The reversible reduction potentials of TCNE and $IrCl_6^{2-}$ in acetonitrile are 0.46 and 0.67 volts vs. SHE, respectively. Unfortunately the oxidation potentials of tetraalkyltin and -lead are not experimentally measurable due to the irreversibility of the cyclic voltammograms. However, there is an empirical linear correlation relating E^0_{RM} to I_D of these alkylmetals, i.e.,

$$I_D = 1.8\ E^0_{RM} + \text{constant} \tag{35}$$

which derives from eqs 8 and 9. Thus to evaluate ΔG^0 for various alkylmetals, the absolute measurement of E^0_{RM} is required for only one alkylmetal. We resort again to the comparative method, and arbitrarily set $E^0_{Me_4Sn} = 1.39$ volts to allow:

$$\Delta G^0_{Me_4Sn} = \Delta G^{\ddagger}_{Me_4Sn}\ , \text{ i.e., } w^p_{Me_4Sn} = 0$$

The free energy change ΔG^0 for the other alkylmetals can be derived from eq 35. The difference in work terms designated as Δw^p can be evaluated relative to Me_4Sn, i.e.,

$$\Delta w^p = \Delta\Delta G^{\ddagger} - \Delta\Delta G^0 \tag{36}$$

where $\Delta\Delta G^{\ddagger} = \Delta G^{\ddagger}_{RM} - \Delta G^{\ddagger}_{Me_4Sn}$ and $\Delta\Delta G^0 = \Delta G^0_{RM} - \Delta G^0_{Me_4Sn}$. According to this formulation, steric effects in an inner-sphere mechanism for electron transfer are embodied in the work term.

The work term becomes largely an electrostatic interaction in the charge transfer model for an inner-sphere mechanism. According to Mulliken, the charge transfer transition in eq 24 corresponds to an electronic excitation from the charge transfer (ground state) complex to an excited ion-pair state. The potential energy surfaces are depicted in Figure 14, where the crossing occurs at the transition state for thermal electron transfer. The activation energy E_T for electron transfer can be represented as:

$$E_T = I_D - E_A - e^2/r^{\ddagger} - \Delta E_{solv} \tag{37}$$

where $r^{\ddagger}$ is the mean separation of the ion-pair in the transition state and the solvation terms are collected in ΔE_{solv}. The work term in eq 34 may be ascribed totally to an electrostatic potential, i.e., $w^p = -e^2/r^{\ddagger}$ for the ions, $RM^{\dagger}$ and $TCNE^{\cdot-}$ or $IrCl_6^{3-}$. In solution, this work term must be corrected for solvation, i.e.,

$$w^p = -e^2/r^{\ddagger} + \Delta\Delta H \tag{38}$$

where $\Delta\Delta H$ is the difference in solvation energy of the products and the transition state. Using the comparative method, we define the work term w^p for alkylmetals relative to that of the reference Me_4Sn, i.e.,

$$\Delta w^p = w^p_{RM} - w^p_{Me_4Sn} = -e^2/r^{\ddagger}_{RM} + \Delta\Delta H_{RM} + e^2/r^{\ddagger}_{Me_4Sn} - \Delta\Delta H_{Me_4Sn}$$

If the changes in solvation energies are constant, which is reasonable for a series of

related alkylmetals, then:

$$\Delta w^P = e^2/r^{\ddagger}_{Me_4Sn} - e^2/r^{\ddagger}_{RM}$$

The work term defined by this electrostatic model has the same functional form of ΔE obtained independently in eqs 17 and 29 (where $G_1 = e^2/r_{DA}$) from the charge transfer interaction, i.e.,

$$\Delta E = e^2/r_{Me_4Sn\text{-}TCNE} - e^2/r_{RM\text{-}TCNE}$$

Indeed there is a reasonably good agreement between Δw^P and ΔE for tetraalkyltin and especially for methylethyllead. The general trend of the agreement is unmistakable, and it strongly implies that the mean separation in the charge transfer complex is a factor in the transition state structure, particularly as it relates to steric effects.

The same analysis can be carried out for electron transfer to $IrCl_6^{2-}$, and the agreement between Δw^P and ΔE is also reasonably good. It is noteworthy that the work term for electron transfer between Me_4Sn and TCNE is 4.2 kcal mol^{-1} less than that for Me_4Sn and $IrCl_6^{2-}$. If this difference is wholly attributable to an electrostatic term, a difference of 0.1 Å is required to account for the change in distance [which interestingly is the difference in van der Waals radii of Cl(1.8 Å) in $IrCl_6^{2-}$ and C(1.7 Å) in TCNE].

According to this formulation, the mean separation r_{DA} between the donor and the acceptor provides an important indication of the transition state for electron transfer. A relevant question which now arises is: What happens as r_{DA} continues to shrink? At what point does an electron transfer process become an electrophilic process? The distinction between the two has been recently summarized.(24) These questions will take on further relevance in the ongoing studies(25) of halogen cleavage of alkylmetals in which novel charge transfer spectral bands have been detected and related to halogenolysis—a typical electrophilic process in organometallic chemistry.

We now proceed to a description of other organometallic reactions of the transition metals, in which the same basic concepts outlined in the foregoing sections are applicable.

VII. ORGANOMETALLIC REACTIONS OF NICKEL

Nickel is one of the most useful metals in both organometallic reactions as well as in the catalysis of organic reactions.(26) In this section we have chosen some representative reactions to illustrate the importance of charge transfer interactions as they also apply to organometallic processes of transition metal analogues.

A. Mechanism of Oxidative Addition—The Reaction of Nickel(0) Complexes with Aromatic Halides

The oxidative addition of aryl halides to NiL_4 [where L = PEt_3] affords trans-arylnickel(II) halide **A** together with paramagnetic nickel(I) halides **B** as side products.(27)

$$NiL_4 + ArX \longrightarrow \underset{\mathbf{A}}{ArNiXL_2} + 2L \quad (39)$$

$$NiL_4 + ArX \longrightarrow \underset{\mathbf{B}}{XNiL_3} + Ar\cdot + L \quad (40)$$

Any mechanistic formulation for oxidative addition must accommodate such a simultaneous transformation of nickel(0) to the diamagnetic nickel(II) adduct as well as to the paramagnetic nickel(I) product. Thus, oxidative addition in eq 39 formally represents a two-equivalent change for nickel(0), whereas the nickel(I) product derives from a one-equivalent process involving halogen atom transfer in eq 40. It is possible that these apparently dissimilar transformations proceed via two entirely independent, but parallel pathways represented schematically below (presented without phosphine ligands for emphasis), i.e.,

$$Ni^0 + ArX \longrightarrow \begin{cases} ArNi^{II}X \\ XNi^{I} + Ar\cdot \end{cases}$$

Alternatively, these nickel(I) and nickel(II) products may be derived from a common intermediate, e.g.,

$$Ni^0 + ArX \longrightarrow [Ni^I ArX^{\cdot-}] \longrightarrow \begin{cases} ArNi^{II}X \\ XNi^{I} + Ar\cdot \end{cases}$$

In this discussion we wish to show first how the competition between oxidative addition and

halogen atom transfer provides an important key for unlocking the mechanism of the interaction of these nickel(0) complexes with aryl halides.

Criteria for a Common Intermediate. The evidence for a common intermediate rests firmly on three independent observations. First, substituent effects on the rates of reactions of nickel(0) with aryl iodides are strongly correlated with those of aryl bromides as well as those of aryl chlorides. On the other hand, no such correlation exists for the distribution among nickel(II) and nickel(I) products with the changes in either the halide or the substituent. In other words, changes in the rate-limiting transition states are not directly reflected in a corresponding change of the product distribution. Such circumstances can only pertain if one or more intermediates intervene between reactants and products.

The same conclusion derives from the study of solvent effects. Thus, the relative reactivities of aryl iodides are the same in hexane as in THF, despite a significant increase in rate. On the other hand, the product distributions, i.e., [ArNi(II)]/[Ni(I)], actually show inversions with changes in solvent. Therefore, the rate-limiting activation process cannot lead directly to the nickel(II,I) products.

Finally, the deliberate addition of the paramagnetic nickel(I) complex leads to increased yields of additional nickel(I). However, there is no significant, corresponding change in the rates of reaction as measured by the disappearance of nickel(0). Therefore, the nickel(I) as well as the nickel(II) product must be formed subsequent to the rate-limiting step.

The nature of the common intermediate is readily deduced from the redox properties of the reactants. Thus, the zerovalent triethylphosphine complexes of nickel are strong reducing agents, and cyclic voltammetry in Figure 19 shows that they undergo facile one-

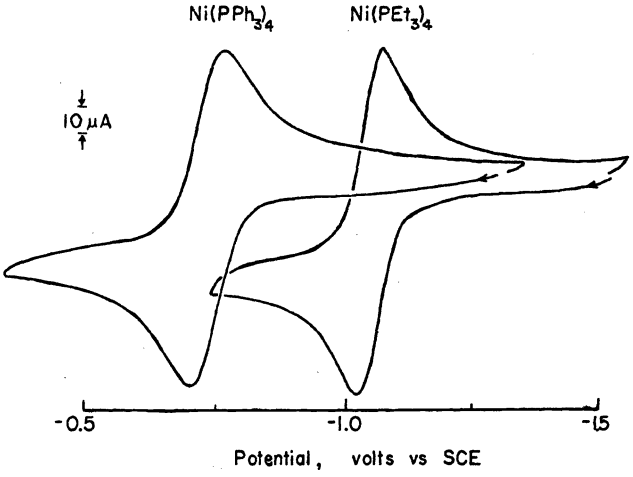

Figure 19. Initial scan cyclic voltammetry in acetonitrile solution of the first anodic wave of: (left) 1.0×10^{-3} M $Ni(PPh_3)_4$ with saturated PPh_3 and (right) 4.5×10^{-4} M $Ni(PEt_3)_4$ with 4.5×10^{-2} M PEt_3.

equivalent oxidations to nickel(I). Similar transformations of nickel(0) occur chemically with a variety of one-electron acceptors, including quinones and cyanoolefins. Likewise, aryl halides are easily reduced electrochemically and they are known to participate effectively as acceptors in electron transfer reactions with donors such as alkali metals, carbanions and organometals. Thus, electron transfer represents a reasonable pathway for the the nickel(0) donor to interact with the electron-deficient aryl halide, i.e.,

$$Ni^0 + ArX \longrightarrow [Ni^I XAr^{\cdot -}] \qquad (41)$$

Accordingly, we formulate the ion pair in eq 41 as the common intermediate which is partitioned between the nickel(II) and the nickel(I) products in the following way:

$$[Ni^I XAr^{\cdot -}] \begin{cases} \longrightarrow ArNi^{II}X \\ \longrightarrow Ni^IX + Ar\cdot \end{cases}$$

To facilitate the discussion, we first present the general mechanism for the reaction of nickel(0) and aryl halides in Scheme IV,

Scheme IV:

$$NiL_4 \underset{}{\overset{K_1}{\rightleftharpoons}} NiL_3 + L \quad (42)$$

$$Ni^0L_3 + ArX \xrightarrow{k_2} [Ni^IL_3\,ArX^{\cdot-}] \quad (43)$$

$$[Ni^IL_3\,ArX^{\cdot-}] \longrightarrow ArNi^{II}XL_2 + L \quad (44)$$

$$[Ni^IL_3\,ArX^{\cdot-}] \xrightarrow{\text{diffuse}} Ni^IL_3 + X^- + Ar\cdot \text{ , etc.} \quad (45)$$

in which L = PEt_3 and the formal oxidation states are included to allow emphasis of the redox changes. According to Scheme IV, the equilibrium formation of the coordinatively unsaturated $Ni(PEt_3)_3$ in eq 42 is followed by the slow rate-limiting electron transfer in eq 43 to afford an ion pair indicated in brackets. Cage collapse affords oxidative adduct in eq 44, which is competitive with diffusion in eq 45. The stability and lifetime of the caged ion pair then determines the product distribution. Each of the important facets of this mechanism will be treated separately below.

(1) Coordinatively Unsaturated $Ni(PEt_3)_3$ as the Reactive Species. The facile dissociation of phosphine from nickel(0) allows essentially three species to be considered for the direct reaction with aryl halides, as outlined below.

$$NiL_4 \underset{}{\overset{K_1}{\rightleftharpoons}} NiL_3 + L \quad (46)$$

$$NiL_3 \underset{}{\overset{K_2}{\rightleftharpoons}} NiL_2 + L \quad (47)$$

$$NiL_4 + ArX \xrightarrow{k_1} \text{products} \quad (48)$$

$$NiL_3 + ArX \xrightarrow{k_2} \text{products} \quad (49)$$

$$NiL_2 + ArX \xrightarrow{k_3} \text{products}$$

The inverse phosphine dependence of the observed second-order rate constant in Figure 20

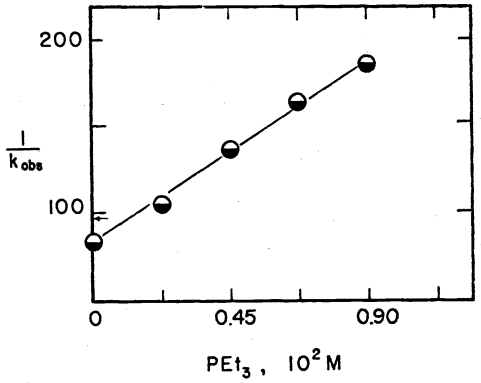

Figure 20. Phosphine dependence of the second-order rate constant for the reaction of 4.16×10^{-3} M bromobenzene and 4.16×10^{-4} M $Ni(PEt_3)_4$ in THF.

can be attributed to the mass law effect in eqs 46 and 47, if either or both of the coordinatively unsaturated species $Ni(PEt_3)_3$ and $Ni(PEt_3)_2$ are directly involved. However, K_2 is at least 10^4 less than K_1, and the simplest formulation would include only eqs 46 and 49, for which the kinetic expression is:

$$-\frac{d[NiL_3]}{dt} = \frac{K_1 k_2}{K_1 + [L]}[NiL_3][ArX] \quad (50)$$

Indeed, the inverse phosphine dependence in Figure 20 shows that the observed second rate constant k_{obs} can be quantitatively expressed as in eq 50.

(2) Electron Transfer as the Rate-Limiting Step. Electrochemical reduction represents a suitable model for the activation process in electron transfer to a series of aryl

halides from $Ni(PEt_3)_3$ according to eq 51. Cyclic voltammetry is a useful technique for examining the reversible formation of the aromatic halide anion-radical:

$$ArX \xrightarrow[(a)]{+e} ArX^{\cdot -} \xrightarrow[(b)]{\tau} Ar\cdot + X^- \qquad (51)$$

which has been identified by its esr spectrum particularly if it has polar substituents. With most aryl halides, however, the anion-radical is too unstable for study (vide infra).

The polarographic half wave potentials of a series of substituted chlorobenzenes, bromobenzenes and iodobenzenes follow a reasonable Hammett plot with a positive slope,(28) consistent with one-electron reduction in eq 51(a). Significantly, the ρ values derived from $E_{1/2}$ are strongly dependent on the halide, increasing in the order: ArI < ArBr < ArCl as $\rho(E_{1/2})$ = +0.26, +0.57 and +0.71, respectively. The same trend in ρ values is obtained from the rates of nickel(0) reaction with aryl halides, which also increase in the order: ArI < ArBr < ArCl as $\rho(k_{Ni})$ = +2.0, +4.4 and +5.4, respectively. The relationship between the electrochemical reduction and the nickel(0) reductions is illustrated in Figure 21.

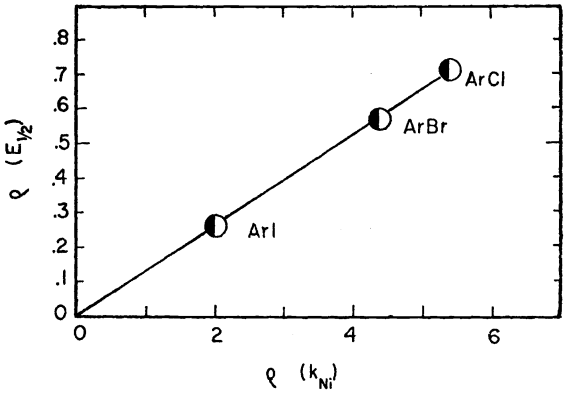

Figure 21. Relationship between the sensitivity of the polarographic half wave potentials for the reduction of a series of substituted chlorobenzenes, bromobenzenes and iodobenzenes with the sensitivity to reaction with $Ni(PEt_3)_4$; plotted as the respective Hammett ρ-values.

The linear correlation in Figure 21 with a slope of 7.7 implies that a strong similarity exists between the transition state for the nickel(0) reaction and the driving force for the electrochemical reduction of aryl halides. Indeed, the plot of the individual rate constants for the nickel(0) reaction in Figure 22 would represent a linear free energy relationship if the polarographic $E_{1/2}$ values represented the reversible reduction potentials of the various aryl halides. Under these circumstances the slope of 8.5 arbitrarily drawn with dashed lines through each of the three sets of points for aryl chlorides, bromides and iodides is that predicted by Marcus theory for an outer-sphere electron transfer process, i.e.,

$$\log k = 8.5\, E^0 + \text{constant} \qquad (52)$$

The first polarographic wave for many simple aryl halides is irreversible, and there are kinetic terms to be included in $E_{1/2}$. The extent to which the kinetic terms may be variable with changes in substituents could obscure the rigorous interpretation of this reaction as an outer-sphere process. Nonetheless, the unmistakable trends in both Figure 21 and 22 establish the importance of electron transfer in the reaction of aryl halides with $Ni(PEt_3)_3$ as depicted in Scheme IV. Such an electron transfer process to afford an ion pair is to be distinguished from one in which electron transfer merely makes a partial contribution to the transition state of a concerted process. Indeed, the formation of this highly ionic product is supported not only by the correlations in Figure 21 and 22 but also the strong dependence on solvent polarity. It is noteworthy that despite the differences in the absolute rate constants for reactions carried out in hexane and in THF, they both show the same sensitivity to polar substituents, and importantly, the slope of the correlation of 1.0 shows that charge development is the same in hexane and in THF, which (barring fortuitous coincidences) can only be readily accounted for by the formulation of ion pairs as actual intermediates.

Our attention is now drawn to the properties of the ion pair, which identify it as the common intermediate leading to oxidative addition or nickel(I) formation.

(3) Ion Pairs as the Common Intermediates--Partitioning to Oxidative Adducts and Nickel(I) Products. According to Scheme IV, the oxidative adduct is formed by the collapse of the tight ion pair in eq 44 which must compete with diffusion of aryl radicals out of

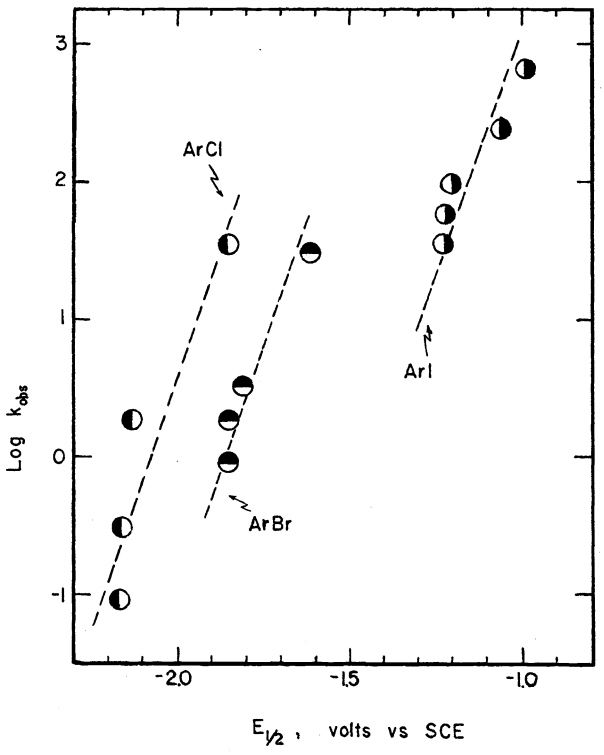

Figure 22. Correlation of the polarographic half wave potentials for the reduction of substituted ◑ iodobenzenes, ◓ bromobenzenes and ◐ chlorobenzenes with the second-order rate constants for reactions with $Ni(PEt_3)_4$. The dashed lines are arbitrarily drawn with slope = 8.5.

the solvent cage. Since such a partitioning of the common intermediate occurs subsequent to the rate-limiting electron transfer step, it can only be considered in the light of product formation. We focus thus on factors involved in (a) the collapse of the ion pair to oxidative adduct and (b) the formation of aryl radicals and nickel(I), using as variable probes the nature of the halide, the nuclear substituents (particularly those with charged poles) and the solvent as discussed individually below.

Cage collapse of the ion pair derives part of its driving force from the formation of the nickel-halogen bond, since the highest yields of oxidative adducts are invariably obtained from aryl chloride > aryl bromides > aryl iodides in accord with the expected metal-halogen bond strengths. Moreover, the absence of any large, systematic effects of (uncharged) nuclear substituents on the yields of oxidative adducts suggests that the stabilization of the aryl moiety is not an important consideration.

The geometry of the ion pair is most likely to be that in which the nickel lies below the plane of the aromatic ring and displaced toward the halide (vide infra). The transition state for insertion stemming from the collapse of such an ion pair is depicted below:

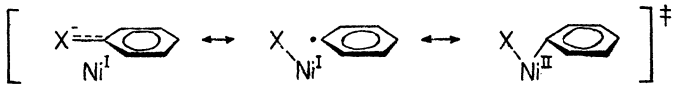

Figure 23. Contributions to the transition state for oxidative addition of aryl halides to $Ni(PEt_3)_3$ by collapse of the ion pair.

The importance of electrostatic effects in the collapse of the ion pair is shown by the significant influence of charged substituents (i.e., poles) on the aromatic nucleus in affecting the yields of oxidative adducts. Thus, unusually high yields of oxidative adducts are formed from aryl halides with negative poles such as p-I-C_6H_4-CO_2^- (88%) and p-I-C_6H_4-$CH_2CO_2^-$ (64%), compared to that obtained from their neutral counterpart, p-I-C_6H_4-CO_2Me (24%). Conversely, the presence of positive poles in p-Br-C_6H_4-NMe_3^+ (38%) and p-Br-C_6H_4-$CH_2NMe_3^+$ (3%) inhibits the formation of oxidative adducts in comparison with that obtained from neutral, uncharged analogs such as p-Br-C_6H_4-CO_2Me (93%) and p-Br-C_6H_4-OCH_3

(89%). Thus, attractive and repulsive electrostatic potentials, represented by aromatic substituents with negative and positive charges, respectively, accord with the ease of collapse of the ion pair to oxidative adduct.

The formation of aryl radicals and nickel(I) derives from a competing homolysis of the $ArX^{-\cdot}$ moiety in the ion pair. Thus, an important feature of the ion pair $[Ni(I)\ ArX^{-\cdot}]$ resides in the stability of the $ArX^{-\cdot}$ moiety which is itself highly prone to spontaneous dissociation. For example, cyclic voltammetry has shown that the half life τ for dissociation in eq 51(b) is strongly dependent on the nature of the halide, and it generally increases in the order: $\tau_X = ArI^{-\cdot} < ArBr^{-\cdot} < ArCl^{-\cdot}$. In particular, for the series of $PhCOC_6H_4X$, the trend in first-order rate constants for the decomposition of the haloaromatic anion-radical has been measured as: p-Br > m-Br > p-Cl to be $10^{4.9}:10^{2.9}:10^{1}\ sec^{-1}$ in dimethylformamide solutions.(29) Similarly, in the series of $O_2NC_6H_4X$, the rates of decomposition of the anion-radical are: p-I > p-Br as $10^{0}:10^{-2.4}\ sec^{-1}$ and o-I > o-Br > o-Cl as $10^{3.9}:10^{2.0}:10^{-2.0}\ sec^{-1}$ in the same solvent.(30) The anion-radicals of the parent halobenzenes are too unstable to observe directly, but a recent indirect approach using homogeneous redox catalysis has provided a lifetime of about 10^{-7} sec for chlorobenzene anion-radical.(31) If the same dissociation of $ArX^{-\cdot}$ applies to that within the ion pair, i.e.,

$$[Ni^{I}\ ArX^{-\cdot}] \longrightarrow [Ni^{I}\ Ar\cdot\ X^{-}]$$

or equivalently:

$$[Ni^{I}\ ArX^{-\cdot}] \longrightarrow [Ni^{I}X\ Ar\cdot]$$

it is expected that the formation of aryl radicals would be the greatest with aryl iodides and the least with aryl chlorides. Indeed, the yields of the nickel(I) side product uniformly increase in the order: ArCl < ArBr < ArI as expected from the trend in stabilities of the anion-radicals.

Thus, the partitioning of the ion pair between oxidative adduct and nickel(I) products can be readily represented by the competition between cage collapse and spontaneous fragmentation of the $ArX^{-\cdot}$ moiety, as elaborated above. However, the phosphine stoichiometry for the two processes differs, i.e., the oxidative adduct $ArNiXL_2$ is formed with loss of one phosphine ligand whereas all three phosphine ligands remain intact on the nickel(I) product, $XNiL_3$. The former may occur simultaneously with (or subsequent to) the collapse of the ion pair in eq 44. However, it is also possible that phosphine loss precedes the collapse of the ion pair, i.e.,

$$[NiL_3^{+}\ ArX^{-\cdot}] \xrightarrow{-L} [NiL_2^{+}\ ArX^{-\cdot}] \longrightarrow ArNiXL_2$$

If so, it may provide yet another factor in the partitioning of the ion pair between oxidative adduct and nickel(I) product.

B. Mechanism of Biaryl Formation from Arylnickel(II) Halides

The arylnickel(II) halides described above are intermediates in the formation of biaryls in the reductive coupling of aryl halides with nickel(0) complexes.(32) As such, the mechanism by which arylnickel(II) halides decompose is relevant. Thermally they are stable, but in the presence of aryl halides they undergo facile decomposition, according to the overall stoichiometry:

$$ArNiBrL_2 + ArBr \longrightarrow ArAr + (ArL)_2NiBr_4 \qquad (53)$$

The stoichiometry for the formation of biaryls and arylphosphonium salts in eq 53 can be represented by three separate transformations:

$$ArNiBrL_2 + ArBr \longrightarrow ArAr + NiBr_2L_2$$

$$NiBr_2L_2 + 2\,ArBr \longrightarrow 2\,ArL^{+}Br^{-} + NiBr_2$$

$$NiBr_2 + 2\,Br^{-} \longrightarrow NiBr_4^{2-}$$

where $L = PEt_3$. From a mechanistic point of view, biaryl and arylphosphonium salts are largely derived from separate processes since scrambling is observed in the biaryls, whereas $ArPEt_3^{+}$ is formed specifically from the aryl halide. However, the two processes are intimately related—they both take place simultaneously, and only immediately after the cessation of the induction period. Indeed, the observations of aryl scrambling and an induction period together provide rare insight into the mechanism of biaryl formation, and they allow us to focus on the delineation of this problem first.

1. Scrambling of Aryl Groups in the Biaryls. The reaction of phenylnickel(II) halide with another aryl halide leads to extensive scrambling of the phenyl groups in the biaryl

fraction, as shown by the use of an o-methoxy group as the label [Ar = o-$CH_3OC_6H_4$], i.e.,

$$\begin{matrix} L \\ | \\ PhNiBr \\ | \\ L \end{matrix} + ArBr \longrightarrow \left.\begin{matrix} \text{Ph-Ph (33\%)} \\ \text{Ph-Ar (44\%)} \\ \text{Ar-Ar (23\%)} \end{matrix}\right\} + (ArL)_2NiBr_4 \qquad (54a)$$

Although extensive, the scrambling is not complete since reversing the label does not quite produce the equivalent results:

$$\begin{matrix} L \\ | \\ ArNiBr \\ | \\ L \end{matrix} + PhBr \longrightarrow \left.\begin{matrix} \text{Ph-Ph (11\%)} \\ \text{Ph-Ar (73\%)} \\ \text{Ar-Ar (16\%)} \end{matrix}\right\} + (PhL)_2NiBr_4 \qquad (54b)$$

Indeed, the trend is for more scrambling to occur with increasing reactivity of the arylnickel(II) complexes.

2. The Rates of Decomposition of Arylnickel(II) Halides Induced by Aryl Halides. The kinetic behavior of the decomposition shows two distinct and unique phases: (a) an induction period followed by (b) a rapid second-order reaction, as described separately below.

(a) Promotion and Removal of the Induction Period. When a clear, homogeneous brown solution of arylnickel(II) halide and aryl halide in benzene is heated at 70°C, there is no apparent change for variable lengths of time, depending on the aryl halide, the arylnickel(II) complex, the temperature and the purity of the reactants. During this quiescent period, there is also no change in the proton nmr spectrum of the solution. As the heating is continued, the solution gradually becomes opalescent, and changes in the nmr spectrum are clearly discernible. The induction period could be deliberately lengthened by adding less than 0.2% of triethylphosphine. The presence of large amounts of phosphine inhibited the reaction completely. Control experiments showed that triethylphosphine did not separately react with either arylnickel(II) halide or aryl halide to any detectable extent under these reaction conditions. Conversely, the induction period could be shortened considerably by adding small amounts of either nickel bromide (heterogeneous) or methyl trifluoromethanesulfonate. It is striking that as chemically dissimilar as nickel bromide and methyl trifluoromethanesulfonate are, they both effectively serve a common function in this system. Indeed, nickel bromide is so insoluble in benzene, the amount actually in solution could not be measured. Nonetheless, even under these conditions, it can coordinate with triethylphosphine:

$$NiBr_2 + 2\,PEt_3 \longrightarrow NiBr_2(PEt_3)_2$$

In a similar vein, methyl trifluoromethanesulfonate readily alkylates triethylphosphine:

$$CH_3OSO_2CF_3 + PEt_3 \longrightarrow CH_3PEt_3^+\,CF_3SO_3^-$$

Thus, these reactions are effective in the removal of free triethylphosphine extant in solution, and both can be considered as "phosphine traps."

(b) Kinetics. Following the induction period, the decomposition of the arylnickel(II) complex in Figure 24 proceeded with pseudo first-order kinetics,

$$-\frac{d[ArNiXL_2]}{dt} = k_{obs}[ArNiXL_2]$$

where $k_{obs} = k_2[ArX]$. Significantly, the apparent rate constant of $k_{obs} = 1.23 \times 10^{-3}$ sec^{-1} was the same as that obtained from the phosphine-inhibited reaction with $k_{obs} = 1.18 \times 10^{-3}$ sec^{-1}. Furthermore, the same rate constant was observed in those reactions promoted by nickel bromide and by methyl triflate. One can conclude from these results that these additives, independent of whether they shorten or extend the induction periods, are not directly involved in decomposition itself.

The rate constants for decomposition of o-anisylnickel(II) bromide in the presence of various substituted phenyl bromides are plotted against the Hammett σ-constant in Figure 25, showing $\rho \sim 1$.

3. Probes for Chain Reactions and Radical Intermediates. The dual observations of induction periods and aryl scrambling are symptomatic of radical chain reactions and aryl radicals as intermediates, as described below.

Inhibition of Radical Chain Processes. The participation of radical chain processes was examined with three types of inhibitors: nitroaromatic and quinones, oxygen and stable radicals. However, it could be shown that aryl radicals are not the reactive paramagnetic

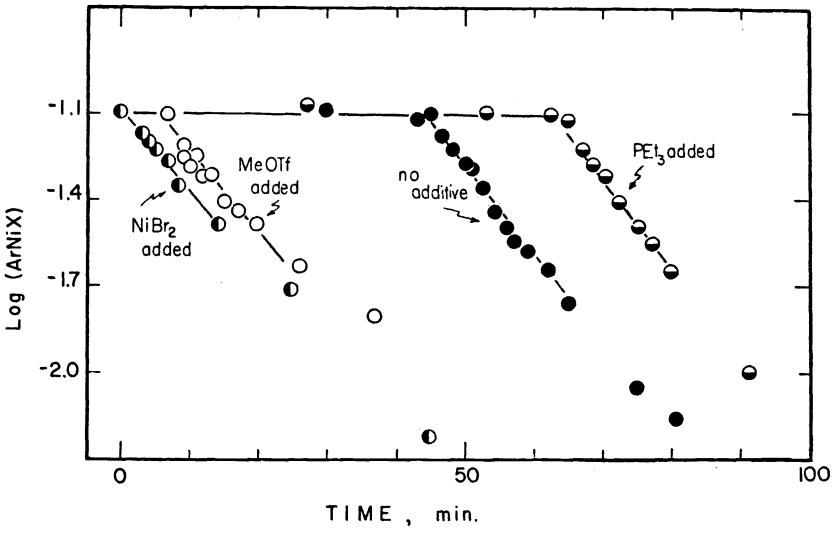

Figure 24. Radical chain mechanism for the decomposition of 0.08 M o-anisylnickel(II) bromide and 1.6 M iodobenzene in benzene solution at 55°C. Effect of additives: ◐ $NiBr_2$, O methyl triflate, ◒ 0.2% PEt_3, ● none.

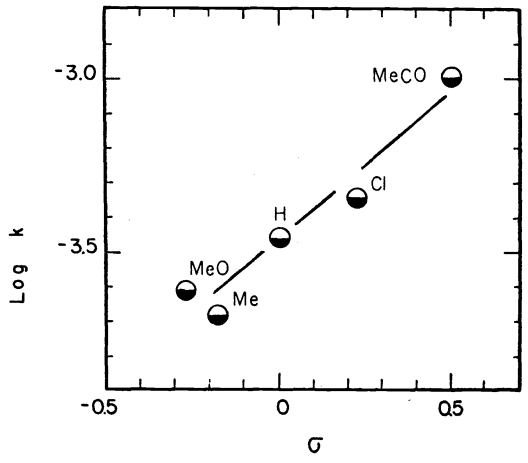

Figure 25. Hammett correlation of the rates of reaction of o-anisylnickel(II) bromide with para-substituted bromobenzenes in benzene solution at 80°C.

intermediates responsible for the chain decomposition. Thus tolyl radicals generated independently,

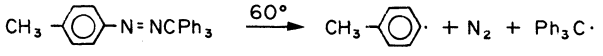

had no effect on the course of reaction. In the absence of aryl radicals as viable intermediates, we turn to other reactive intermediates which could promote aryl scrambling and aryl exchange with the initial arylnickel(II) halide. The rather selective inhibition by electron acceptors such as quinones and nitroaromatics suggests that ion-radicals such as nickel(I) and nickel(III) are intermediates, reminiscent of a similar observation in the alkylation of π-allylnickel(II) halides with alkyl and vinylic halides. Such paramagnetic species as arylnickel(III) species, for which there is recent independent evidence, are included as key reactive intermediates in the propagation steps for the chain process shown below.

Scheme V:

$$Ni^{I}X + ArX \longrightarrow ArNi^{III}X_2 \quad (55)$$

$$ArNi^{III}X_2 + ArNi^{II}X \longrightarrow Ni^{II}X_2 + ArNi^{III}X \quad (56)$$
(Ar)

$$ArNi^{III}X \longrightarrow ArAr + Ni^{I}X \text{ , etc.} \quad (57)$$
(Ar)

According to Scheme V, biaryls result in eq 57 from the reductive elimination of a metastable diarylnickel(III) species, which is formed by aryl transfer in eq 56. Oxidative addition of aryl halide to nickel(I) in eq 55 completes the cycle. Indeed, the formulation of nickel(I) and arylnickel(III) species in a chain process provides a consistent basis for explaining all the diverse phenomena observed in this system. Each of these facets will be described separately.

Scrambling of Aryl Groups--Ligand Exchange Process. The aryl halide enters the cycle via oxidative addition to nickel(I) halide in eq 55. The resultant arylnickel(III) dihalide is to be distinguished from the reactant, arylnickel(II) halide, insofar as it contains an additional halogen atom. Since such a paramagnetic species is expected to be labile, it is susceptible to transfer of an aryl ligand as in eq 56. Alternatively, transfer of halogen as depicted below:

$$ArNi^{III}X_2 + ArNi^{II}X \longrightarrow ArNi^{II}X + ArNi^{III}X_2 \quad (58)$$

is tantamount to aryl transfer, although it occurs without actual rupture of the Ar-Ni bond. Furthermore, halogen transfer in eq 58 scrambles aryl groups between nickel(II) and nickel(III) without causing a simultaneous aryl exchange.

Aryl transfer and halogen transfer in eqs 56 and 58, respectively, are formally considered to be electron transfer reactions between nickel(II) and nickel(III) centers. As such, they are to be included in the well-known class of ligand transfer processes in which there are established examples of halo and aryl groups as bridging ligands. The transition state (or intermediate) for such an inner-sphere process can be depicted as the singly or doubly bridged structures below:

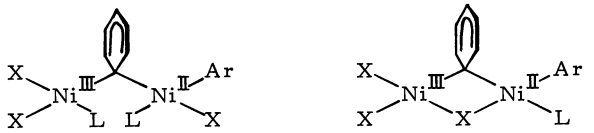

Although aryl radicals and halogen atoms are not explicitly included as reactive intermediates in such a formulation, their effectiveness as bridging ligands is reflected in the facility with which they are transferred. Viewed in this way, cross coupling and scrambling in biaryl formation actually represent competing processes for aryl and halogen transfer in eqs 56 and 58, respectively. Indeed, the available data can be interpreted in this regard. Thus, the observation that the extent of aryl scrambling decreases in the order: I > Br, is consistent with their relative abilities to serve as bridging ligands. Similarly, a more facile aryl transfer would lead to biaryls with higher specificity for cross coupling and less aryl scrambling, in those systems employing a single halogen. Judging from the conjugate pairs of reactions in eqs 54a and b, the presence of an o-methoxy substituent retards aryl transfer since more scrambling occurs in the reaction of o-anisyl bromide with phenylnickel(II) than with phenyl bromide and o-anisylnickel(II).

An inner-sphere complex or transition state as depicted above requires coordinative unsaturation at a nickel center. Indeed, the extremely high susceptibility of biaryl coupling to the presence of triethylphosphine suggests that its coordination in these structures [where L = PEt_3] may influence not only the extent of scrambling but also biaryl formation.

The Initiation Process. According to Scheme V, an arylnickel(III) species is responsible for the initiation of the catalytic cycle. Such a paramagnetic species may be formed directly from the diamagnetic reactants by an intermolecular electron transfer process, since it can be shown independently that the arylnickel(II) halide is oxidized and the aryl halide is reduced in one-equivalent transformations, as described below.

The oxidation of arylnickel(II) halides is shown by the electrochemical studies at platinum electrodes. The process is a one-electron oxidation,

$$ArNi^{II}X \xrightarrow{-e} ArNi^{III}X \quad (59)$$

although the anodic wave in the cyclic voltammogram is irreversible even at sweep rates greater than 1 volt sec^{-1}, which is consistent with electron transfer followed by a rapid

chemical reaction. Arylnickel(II) halide is also readily oxidized by a variety of one-equivalent oxidants such as hexachloroiridate(IV), cerium(IV) and cobalt(III) trifluoroacetates.(33) If the reaction of $o\text{-}CH_3C_6H_4NiBr(PEt_3)_2$ is carried out at -50°C, the absorption spectrum of a new species, stable at this temperature and absorbing at λ_{max} = 410 nm, can be observed independent of whether Na_2IrCl_6, $Ce(TFA)_4$ or $CuBr_2$ is employed as the oxidant. The same reactions carried out directly in the cavity of an esr spectrometer afforded an intense spectrum with g = 2.196 immediately upon mixing. We ascribe these spectral changes to the same paramagnetic arylnickel(III) species in eq 59 formed by anodic oxidation.

The electrochemical reduction of aryl halides proceeds by a similar EC process in which electron transfer is followed by a rapid, spontaneous fragmentation of the anion-radical, as described above in eq 51. The ease of intermolecular electron transfer between arylnickel(II) halide with various aryl halides, thus,

$$ArNi^{II}X + ArX \longrightarrow ArNi^{III}X + ArX^{\cdot -} \text{ , etc.} \qquad (60)$$

should follow the trend in their reduction potentials, i.e., ArI > ArBr > ArCl. Indeed, induction periods which follow the order: ArI < ArBr < ArCl, parallel the expected relative rates of electron transfer in eq 60. However, the magnitude of the driving force for electron transfer is not expected to be large, since neither is an exceptional electron donor or acceptor, as reductants and oxidants go. As a result, electron transfer is likely to be an inner-sphere process, as shown for a related example in Scheme IV. By analogy, electron transfer from arylnickel(II) halide is expected to proceed via a similar coordinatively unsaturated species, i.e.,

$$ArNiX(PEt_3)_2 \overset{K_1'}{\rightleftharpoons} ArNiX(PEt_3) + PEt_3$$

$$ArNiX(PEt_3) + ArX \xrightarrow{k_{et}'} ArNi^{III}X(PEt_3) + ArX^{\cdot -} \text{ , etc.} \qquad (61)$$

Such a mechanism provides a ready explanation for the unusual and marked dependence of the induction period on the availability of phosphine.

Oxidative Addition of Aryl Halides to Nickel(I) During the Propagation Cycle. According to Scheme V, the aryl halide enters the propagation cycle by effecting oxidative addition to nickel(I) species in eq 55. Indeed, the positive Hammett ρ-value of about one in Figure 25 accords with electron accession to the metal center generally required for such an oxidative addition process. It is noteworthy, however, that the magnitude of ρ in this example is substantially less than ρ = 5.4 for oxidative addition to nickel(0) in eq 43.

Reductive Coupling of Arylnickel(III) Intermediates During the Propagation Cycle. The efficiency of the sequence of propagation steps in Scheme V also depends critically on the rate of reductive elimination of biaryl in eq 57. In accord with this expectation, the anodic oxidation of the diarylnickel(II) complex, $(o\text{-}CH_3C_6H_4)_2Ni(PEt_3)_2$, affords high yields of biaryl, presumably via a diarylnickel(III) intermediate.

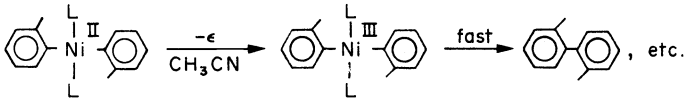

The much slower thermal decomposition of diarylnickel(II) also affords biaryl in essentially quantitative yields. Reductive coupling probably obtains,

$$\begin{matrix} PEt_3 \\ | \\ ArNiAr \\ | \\ PEt_3 \end{matrix} \xrightarrow{\Delta} Ar_2 + [Ni(PEt_3)_2]$$

as qualitatively indicated by the change in color of the solution from yellow to deep brown, suggestive of the presence of unsaturated nickel(0) species. Crossover experiments indicate that the elimination process is intramolecular. Thermolysis as described above, however, is too slow to account for biaryl formation in this system. As expected, addition of bromobenzene considerably enhances the rate of coupling biaryl formation, and it is accompanied by aryl scrambling in basic accord with the mechanism in Scheme V.

Inhibition of the Chain Process. The effectiveness of quinones and nitroaromatics as inhibitors is most easily reconciled with the oxidation of nickel(I) species in Scheme V, since these compounds are known to be effective one-electron acceptors.(34) The less efficient inhibition by the stable radicals, DPPH and galvinoxyl, may be related to the slower rates of oxidation of nickel(I).

Oxygen is a more complex inhibitor since arylnickel(II) halide as well as aryl halide are consumed during the induction period. A complex series of reactions involving autoxi-

dation of phenylnickel(II) halide and further reaction of peroxynickel species are likely to be involved.

C. Mechanism of Oxygen Atom Transfer from Nitro Compounds Mediated by Nickel(0) Complexes

Phosphinenickel(0) complexes NiL_4 react readily with a variety of aliphatic and aromatic nitro compounds RNO_2 to afford the corresponding nitrosonickel(0) complexes $(RNO)NiL_2$ and the phosphine oxide in high yields,(35) e.g.,

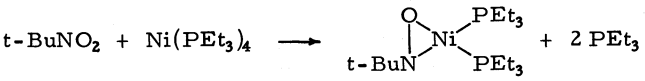

(62)

Kinetic studies show that the coordinatively unsaturated NiL_3, formed by phosphine dissociation, is involved in the rate-limiting reaction with RNO_2, similar to that described above for the oxidative addition of aryl halides in eqs 49 and 61.

The polar effects of the nitro compounds as measured by the Taft σ^* parameters for alkyl groups and the Hammett σ constants for aryl groups correlate directly with their reactivity in oxygen transfer ($\rho = +3.2$). A rate-limiting transition state which is highly polar is also indicated by the linear relationship between the second-order rate constants (i.e., log k_e) and the electrochemical reduction potential E of the nitro compound with a slope, $\alpha = 7$, closely approaching the theoretical limit in eq 52 predicted by Marcus theory for outer-sphere electron transfer to afford the ion pair $[L_3Ni(I)\ RNO_2^{\cdot-}]$. Collapse of such a species to a cyclic intermediate as included in the mechanism below:

Scheme VI:

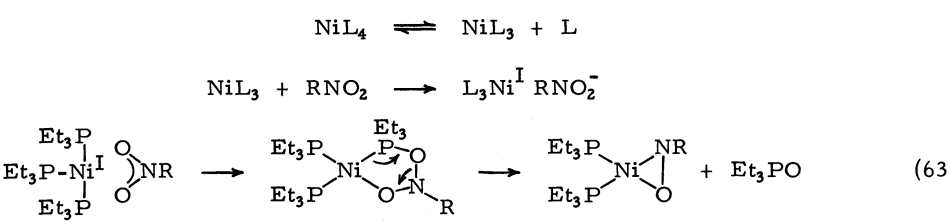

(63)

would allow the direct elimination of phosphine oxide and concomitant formation of the nitrosonickel(0) complex.

D. Mechanism of the Formation of π-Complexes of Nickel(0) with Benzophenones

Upon the addition of one equivalent of benzophenone, the band at 500 nm disappeared with the concomitant growth of a new band at 330 nm. A red crystalline product could be isolated from this solution.(36)

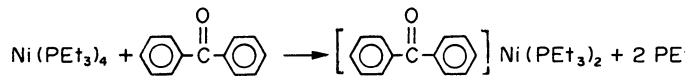

(64)

The formation of the π-nickel(0) complex obeys apparent second-order kinetics, being first-order in $Ni(PEt_3)_3$ and benzophenone according to the equation below:

$$-\frac{d[NiL_3]}{dt} = k_{obs}[ArX][NiL_3]$$

where $L = PEt_3$. The observed second-order rate constant, however, is diminished by added triethylphosphine. Quantitatively the inverse phosphine dependence of the observed rate constant is given by:

$$\frac{1}{k_{obs}} = \frac{1}{k}\left\{1 + \frac{[PEt_3]}{K}\right\} \qquad (65)$$

The value of the phosphine-independent rate constant $k = 22.2\ M^{-1}\ sec^{-1}$ obtained from the intercept affords a value of $K = 4.2 \times 10^{-3}$ M derived from the slope.

Such a relationship for the phosphine dependence would obtain if the 3-coordinate nickel(0) were the species directly involved in π-complex formation.

Scheme VII:

$$NiL_4 \overset{K_1}{\rightleftharpoons} NiL_3 + L \tag{66}$$

$$NiL_3 + Ar_2C{=}O \xrightarrow{k_2} (Ar_2C{=}O)NiL_2 + L \tag{67}$$

The kinetics of π-complex formation according to the mechanism in Scheme VII is given by the rate equation in eq 68, if the phosphine dissociation in eq 66 is fast,

$$\frac{-d[NiL_3]}{dt} = \frac{K_1 k_2}{K_1 + [L]}[Ar_2CO][NiL_3] \tag{68}$$

where $k_{obs} = K_1k_2/\{K_1 + [L]\}$, the inverse of which is equivalent to eq 65, where $k = k_2$ and $K = K_1$. Indeed, $K_1 = 4.2 \times 10^{-3}$ M, independently evaluated by a spectral technique, is the same as that determined kinetically from eq 65.

The effect of polar, nuclear substituents on the rate of π-complex formation Hammett correlation of the second-order rate constants for substituted benzophenones with $\rho = +2.0$ is illustrated in Figure 26. These rate constants (log k_{obs}) are also linearly related to the reduction potentials of the corresponding substituted benzophenones with a slope $\alpha = 5.5$ (compare eq 52). In both cases, the rate of π-complex formation is accelerated by relatively electron-deficient benzophenones and retarded by electron-rich benzophenones, indicating a highly polarized transition state, i.e., $[Ar_2CO^- NiL_3^+]^{\ddagger}$.

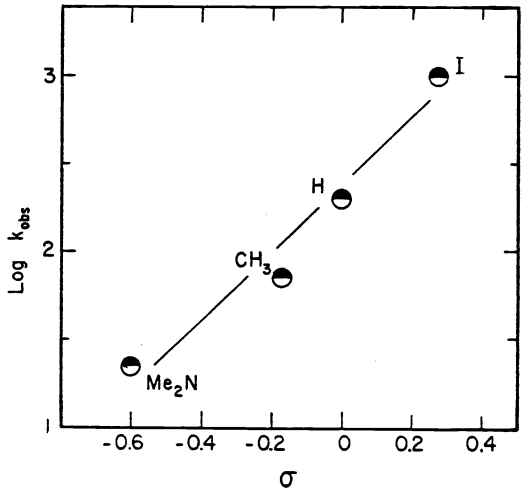

Figure 26. The Hammett correlation of the rate of π-complex formation from $Ni(PEt_3)_4$ and substituted benzophenones.

In summary, all the reactions of nickel(0) complexes which we have studied here involve either a charge transfer process as the rate-limiting step, or one in which a large component of electron transfer pertains, as indicated by the slope α of the Marcus theory (compare eq 52). It is revealing that even a simple substitution process, as in the incorporation of benzophenone in eq 67, is governed by such a charge transfer interaction.

VIII. CONCLUSION

The twin, related concepts of electron transfer and charge transfer can be readily developed in organometallic chemistry, since organometals are excellent electron donors. There is no mechanistic distinction between organometals of the main group elements and those of the transition metals, both readily acting as electron donors with a variety of electron acceptors. Indeed the identification of the latter provides a unifying theme to the rational formulation of mechanisms of the diverse reactions presented in the Introduction to this presentation.

Acknowledgment - I wish to thank my colleagues, especially S. Fukuzumi, C. L. Wong, W. A. Nugent and T. T. Tsou, for their creative and diligent efforts, the National Science Foundation and the Petroleum Research Fund of the American Chemical Society for financial support of this research.

REFERENCES

1. (a) W. V. Steele, Ann. Rep. Chem. Soc. A71, 103 (1974).
   (b) J. A. Connor, Topics Curr. Chem. 71, 71 (1977).
2. T. P. Fehlner, J. Ulman, W. A. Nugent and J. K. Kochi, Inorg. Chem. 15, 2544 (1976).
3. S. Evans, J. C. Green, P. J. Joachim, A. F. Orchard, D. W. Turner and J. P. Maier, J. Chem. Soc., Faraday Trans. II, 905 (1972).
4. C. L. Wong, K. Mochida, A. Gin, M. A. Weiner and J. K. Kochi, J. Org. Chem., submitted for publication.
5. G. Beltram, T. P. Fehlner, K. Mochida and J. K. Kochi, J. Electron Spectrosc., in press.
6. J. H. D. Eland, Int. J. Mass Spectrosc. Ion Phys. 4, 37 (1970).
7. J. L. Franklin and P. W. Harland, Ann. Rev. Phys. Chem. 25, 485 (1974).
8. J. K. Kochi, Organometallic Mechanisms and Catalysis, Academic Press, New York, 1978.
9. (a) J. Y. Chen and J. K. Kochi, J. Am. Chem. Soc. 99, 1450 (1977).
   (b) S. Komiya, unpublished results.
10. J. Halpern, M. S. Chan, J. Hanson, T. J. Roche and J. A. Topich, J. Am. Chem. Soc. 97, 1606 (1975).
11. M. Alemark and B. Akermark, J. Chem. Soc., Chem. Commun., 66 (1978). See also ref 13.
12. S. Komiya, T. A. Albright, R. Hoffmann and J. K. Kochi, J. Am. Chem. Soc. 99, 8440 (1977).
13. T. T. Tsou and J. K. Kochi, J. Am. Chem. Soc. 100, 1634 (1978).
14. For listings of electron affinities see G. G. Christophorou, Atomic and Molecular Radiation Physics, Wiley-Interscience, New York, 1971.
15. (a) Compare R. E. Dessy and L. A. Bares, Acc. Chem. Res. 5, 415 (1972).
   (b) W. Tochterman, Angew. Chem. Int. Ed. 5, 351 (1966).
   (c) G. Wittig, Quart. Revs. 20, 191 (1966).
   (d) J. F. Normant, Synthesis, 63 (1972).
   (e) A. Tamaki and J. K. Kochi, J. Chem. Soc., Dalton Trans., 2620 (1973).
   (f) D. G. Morrell and J. K. Kochi, J. Am. Chem. Soc. 97, 7262 (1975).
16. C. L. Wong and J. K. Kochi, J. Am. Chem. Soc., in press.
17. C. Walling and R. A. Johnson, J. Am. Chem. Soc. 97, 2405 (1975).
18. A. A. Schilt, Analytical Applications of 1,10-Phenanthroline and Related Compounds, Pergamon Press, 1969.
19. (a) N. A. Clinton, H. C. Gardner and J. K. Kochi, J. Organometal. Chem. 56, 227 (1973).
   (b) N. A. Clinton and J. K. Kochi, J. Organometal. Chem. 56, 243 (1973).
20. J. Y. Chen, H. C. Gardner and J. K. Kochi, J. Am. Chem. Soc. 98, 2460 (1976).
21. S. Fukuzumi, K. Mochida and J. K. Kochi, J. Am. Chem. Soc., in press.
22. S. Fukuzumi, C. L. Wong and J. K. Kochi, J. Am. Chem. Soc., submitted for publication.
23. R. A. Marcus, J. Phys. Chem. 72, 891 (1968).
24. See p. 563 ff in ref 8.
25. S. Fukuzumi, unpublished results.
26. P. W. Jolly and G. Wilke, The Organic Chemistry of Nickel, Vol. 1 and 2, Academic Press, New York, 1975.
27. T. T. Tsou and J. K. Kochi, J. Am. Chem. Soc., in press.
28. J. W. Sease, F. G. Burton and S. L. Nickol, J. Am. Chem. Soc. 90, 2595 (1968).
29. L. Nadjo and J. M. Saveant, J. Electroanal. Chem. 30, 41 (1971).
30. W. C. Danen, T. T. Kensler, J. G. Lawless, M. F. Marcus and M. D. Hawley, J. Phys. Chem. 73, 4389 (1969); P. P. Van Duyne and C. N. Reilley, Anal. Chem. 44, 158 (1972).
31. C. P. Andrieux, J. M. Dumas-Bochiat and J. M. Saveant, J. Electroanal. Chem. 88, 43 (1978).
32. T. T. Tsou and J. K. Kochi, J. Am. Chem. Soc., in press.
33. T. T. Tsou and J. K. Kochi, J. Am. Chem. Soc. 100, 1634 (1978).
34. N. Kornblum, Angew. Chem. Int. Ed. 14, 734 (1975) and related papers.
35. R. S. Berman and J. K. Kochi, Inorg. Chem., in press.
36. T. T. Tsou and J. K. Kochi, Inorg. Chem. 18, 2311 (1979).